Equilibrium theory of ion exchange chromatography with variable solution normality and steric hindrance

M. Fechtner[a], A. Kienle[a,b,*]

[a] *Otto-von-Guericke-Universität, Universitätsplatz 2, D-39106 Magdeburg, Germany*
[b] *Max-Planck-Institut für Dynamik komplexer technischer Systeme, Sandtorstrasse 1, D-39106 Magdeburg, Germany*

Abstract

The paper extends equilibrium theory of ion exchange chromatography to account for variable solution normality and steric hindrance. Both effects are crucial for many separations including the separation of proteins. Analytical solutions are given for a full chromatographic cycle consisting of the loading of an empty bed equilibrated at different salt concentrations followed by a regeneration step. Special emphasis is on selectivity reversals. It is shown that additional reversals may occur due to a change in solution normality. Results are illustrated step by step and relation to ion exchange chromatography with constant solution normality and/or mass action equilibrium without steric hindrance is discussed. Theoretical findings are validated by comparison with numerical simulation.

Keywords: Ion Exchange, Chromatography, Solution Normality, Steric Hindrance, Equilibrium Theory, Selectivity Reversal

1. Introduction

Equilibrium theory is a powerful method for understanding and designing chromatographic processes [1, 2, 3, 4, 5]. It assumes thermodynamic equilibrium

*Author to whom all correspondence should be addressed.
Email address: kienle@mpi-magdeburg.mpg.de (A. Kienle)

between the solid and the fluid phase leading to a system of first order partial differential equations, which admits analytical insight into propagating concentration fronts and pulses in a chromatographic column. Patterns of behavior crucially depend on the adsorption mechanism, which is represented by the adsorption isotherm. An important class of processes is based on ion exchange chromatography. Classical equilibrium theory for stoichiometric ion exchange is for mixtures with equal valences leading to explicit adsorption isotherms similar to the well known Langmuir isotherm [1]. In contrast to this, unequal valences lead to implicit adsorption isotherms that were studied by Tondeur [6, 7] with special emphasis on selectivity reversals, which may occur for mixtures with unequal valences. A summary was given by Helffereich and Klein in [1]. Missing aspects of the theory were added recently in [8] and an analytical solution of the full chromatographic cycle was given comprising the loading of an empty bed followed by a subsequent regeneration. In this paper also a reformulation strategy has been proposed to provide an efficient numerical solution using standard methods for differential algebraic equation (DAE) systems.

All of these approaches assume constant ionic strength and neglect steric effects. However, variable ionic strength plays an important role in gradient and displacement chromatography, which are frequently applied to enhance the separation of molecules with similar properties [9, 10, 11]. Further, steric effects play an important role for larger molecules such as proteins encountered in many bio separations [12, 13]. Therefore, the objective of the present paper to extend equilibrium theory for stoichiometric ion exchange to processes with variable ionic strength and to account for steric effects by using the well known steric mass action law (SMA) [14]. Consequently, the extension in this paper inherits also the limiting assumptions of the SMA, most notably the lack of accounting for a variation in pH or a variable exchanger capacity based on the dissociation of weak acid functional groups in the solid phase. Contributions that provide a local equilibrium model for these cases, which are not considered here, are for example [15] and [16], respectively.

Past attempts to apply the method of characteristics in ion exchange chro-

matography using the SMA were performed in [9] for binary mixtures and isocratic elution as well as in [17] for binary mixtures and linear salt gradients. Further extensions of the equilibrium theory to ternary systems for monovalent species [18] or related to step gradient conditions [19] for binary mixtures were also presented. However, past contributions do not provide the rigorous application of the equilibrium theory to arbitrary N component systems using the SMA with variable solution normality.

In the following, the theory is developed step by step, and the relation to the previous findings for systems with constant solution normality and mass action equilibria without steric hindrance is established. For illustration purposes of the different effects, three different application examples are considered afterwards. Analytical results are validated through comparison with numerical simulation.

2. Model Equations

The following is based on the well-known ideal model of chromatography

$$\frac{\partial}{\partial t}\left(\mathbf{c}+F\mathbf{q}(\mathbf{c})\right)+\frac{\partial \mathbf{c}}{\partial z}=0, \qquad \mathbf{c},\mathbf{q}\in R^N. \tag{1}$$

It assumes isothermal operation, thermodynamic equilibrium between the adsorbed and the fluid phase, a constant interstitial velocity u of the fluid phase, a constant void fraction ϵ, and it neglects axial dispersion. The parameter $F=(1-\epsilon)/\epsilon$ denotes the phase ratio, and the variables $t=t^*u/L$ and $z=z^*/L$ denote the dimensionless time and space coordinate, respectively, where L is the length of the column. Note that the corresponding dimensionless interstitial velocity in (1) has a value of one. In these model equations, $\mathbf{c}$ represents the concentrations of the N adsorbable components in the fluid phase and $\mathbf{q}(\mathbf{c})$ the corresponding concentrations in the adsorbed phase, which follow from the adsorption equilibrium.

For constant solution normality in system (1) only $N-1$ concentrations are independent, and (1) can be reduced to a system of $N-1$ equations by

introducing dimensionless concentration measures (see e.g. [8]). For variable solution normality, all N concentrations are independent and the full set of equations (1) has to be considered. Therefore a conversion to dimensionless concentration measures is not used in this paper.

The adsorption isotherm of stoichiometric ion exchange follows from the mass action law according to

$$K_{iN} = \left(\frac{q_i}{c_i}\right)^{\nu_i} \left(\frac{c_N}{q_N}\right)^{\nu_N} = const., \qquad i = 1, \ldots, N-1. \tag{2}$$

Following the notation in [8], ν_i is the reciprocal of the characteristic charge of ion 'i', and component 'N' is a suitable reference component. The characteristic charge is assumed to be constant and determines the the multi-pointed binding of larger molecules [14, 20] without accounting for variations in the pH, which is assumed to be constant throughout this paper.

In general component 'N' is usually a simple ionic component. However it can be any kind of reference ion. In order to emphasize its special role in the present paper, component 'N' is denoted as the salt, which is used to change the adsorption behavior of all other components. For constant solution normality $\tilde{c}_{tot}$ the salt concentration is not independent anymore but follows from $c_N = \tilde{c}_{tot} - \sum_{i=1}^{N-1} \frac{c_i}{\nu_i}$, which is not the case in this contribution. Thus, the solution normality can change. Typically, ν_N is equal to one. However, for generality the following development is not restricted to this case. Accordingly, q_N is the salt load of the solid phase or the free accessible salt load of the solid phase in case of steric hindrance by the other molecules. For fixed ion exchanger capacity q_{tot}, the salt load q_N follows from

$$q_{tot} = \sum_{i=1}^{N} \xi_i q_i, \tag{3}$$

$$\xi_i = \frac{1}{\nu_i} + p_i, \tag{4}$$

where p_i accounts for steric effects. For negligible steric effects $p_i = 0$, the corresponding generalized factor ξ_i reduces to $\xi_i = 1/\nu_i$. This applies in particular

to the salt, i.e. $p_N = 0$, also in the presence of steric hindrance by the other molecules. Moreover, the electroneutrality condition is also accounted for by Eq. (3) [14].

In the general case of unequal characteristic charges of the different ions, Eqs. (2), (3) represent a system of implicit algebraic equations, which will be denoted

$$\begin{aligned} 0 &= f_i(\mathbf{q}, \mathbf{c}) = \frac{1}{K_{iN}} \cdot \left(\frac{q_i}{c_i}\right)^{\nu_i} \left(\frac{c_N}{q_N}\right)^{\nu_N} - 1, \quad \forall i = 1, \ldots, N-1, \\ 0 &= f_N(\mathbf{q}) = \sum_{i=1}^{N} \xi_i q_i - q_{tot} \end{aligned} \tag{5}$$

in the following. Additional assumptions required for the SMA are as follows. Equilibrium constants and steric hindrance are also assumed to be constant [14]. Further, the effect of co-ions is neglected based on the assumptions in [20].

For an efficient numerical solution of the model equations we use equations (1) and (5) in combination with the solution strategy introduced in [8] and its extension to the SMA in [21]. This strategy comprises a reformulation of the model equations by introducing variable $\mathbf{v} = \mathbf{c} + F\mathbf{q}(\mathbf{c})$, a discretization of the resulting equations using a method of lines approach [22] with finite differences and a subsequent simultaneous solution of the resulting system of ordinary differential equation applying standard DAE numerics. For demonstration purposes, simple first order backward differences are used based on an equidistant grid with $N_z = 1000$ spatial grid points. The resulting DAE system is solved with ODE15s in MATLAB® [23].

Utilizing the same line of arguments as introduced in [8] and the spectral properties to be discussed in the next section, it can be shown that the differential index of the resulting DAE system is always equal to one [24], which alleviates the numerical solution considerably. For a more detailed discussion of the differential index of DAE systems the reader is also referred to [8] and further references therein.

Finally, it is important to note that instead of the N component material balances of Eq. (1) we may also use only $N-1$ component material balances

together with some sort of total material balance that is obtained through multiplication of the component material balances with factors ξ_i and summation over all components. Introducing

$$c_{tot} = \sum_{i=1}^{N} \xi_i c_i, \tag{6}$$

we find in view of Eq. (3)

$$\frac{\partial c_{tot}}{\partial t} + \frac{\partial c_{tot}}{\partial z} = \mathbf{0}. \tag{7}$$

It should be noted that c_{tot} is *not* the total solution normality, which would be $\sum_{i=1}^{N} c_i/\nu_i$, but some formal equivalent to q_{tot} in Eq. (3). In the remainder c_{tot} is called the modified solution normality. Modification is due to factors p_i as in (3) accounting for steric hindrance. If this steric hindrance is absent, the modified solution normality coincides with the total solution normality, i.e. the latter is simply a special case included in the modified solution normality.

Eq. (7) represents a linear transport equation with constant transport velocity, which is equal to one. Since Eq. (7) is decoupled from the component material balances (1), c_{tot} depends only on the given boundary and initial conditions but not the component material balances. In contrast to this, the component material balances depend on the value of c_{tot} through the equilibrium relations (5), because of

$$c_N = \frac{c_{tot} - \sum_{i=1}^{N-1} \xi_i c_i}{\xi_N}. \tag{8}$$

The alternative model formulation (7) provides useful insight into the solution structures to be discussed in the next section. In view of Eqs. (1) and (7), we find that any step change of the concentrations at the inlet is resolved into $N-1$ transitions with $c_{tot} = const.$ and a single transition 'N' with variable c_{tot}. In other words the kth transitions with $k < N$ takes place on a specific c_{tot} hyperplane defined by (6). Further details will be discussed in the next section.

3. Equilibrium Theory

The system of quasilinear partial differential equations of first order (1) can be solved analytically for piecewise constant initial and boundary (Riemann) conditions using the method of characteristics. For this purpose Eqs. (1) are rewritten in the following form

$$\frac{\partial \mathbf{c}}{\partial t} + \left(\mathbf{I}_N + F \frac{\partial \mathbf{q}}{\partial \mathbf{c}} \right)^{-1} \frac{\partial \mathbf{c}}{\partial z} = 0, \tag{9}$$

where $\mathbf{I}_N$ denotes the $N \times N$ identity matrix.

Solutions of (9) with Riemann boundary and initial conditions consist of smooth and non-smooth transitions. Non-smooth transitions are either shock waves or contact discontinuities [2, 25]. In the following, it will be shown that contact discontinuities are either related to a selectivity reversal or a change of the solution normality.

The characteristic velocity σ_k of a smooth transition follows from the eigenvalues of matrix $(\mathbf{I}_{N-1} + F\frac{\partial \mathbf{q}}{\partial \mathbf{c}})^{-1}$ in (9) according to

$$\sigma_k = \frac{1}{1 + F\lambda_k}. \tag{10}$$

Therein, the λ_k's are the eigenvalues of the Jacobian matrix $\frac{\partial \mathbf{q}}{\partial \mathbf{c}}$. By implicit differentiation of Eq. (5) we find

$$\frac{\partial \mathbf{q}}{\partial \mathbf{c}} = -\left(\frac{\partial \mathbf{f}}{\partial \mathbf{q}} \right)^{-1} \frac{\partial \mathbf{f}}{\partial \mathbf{c}}, \tag{11}$$

with

$$-\frac{\partial \mathbf{f}}{\partial \mathbf{q}} = \begin{bmatrix} diag_{N-1}\left(-\frac{\nu_i}{q_i}\right) & \begin{matrix} \frac{\nu_N}{q_N} \\ \vdots \\ \frac{\nu_N}{q_N} \end{matrix} \\ \begin{matrix} -\xi_1 & -\xi_2 & \dots & -\xi_{N-1} \end{matrix} & -\xi_N \end{bmatrix}, \tag{12}$$

$$-\frac{\partial \mathbf{f}}{\partial \mathbf{c}} = \begin{bmatrix} diag_{N-1}\left(\frac{\nu_i}{c_i}\right) & \begin{matrix} -\frac{\nu_N}{c_N} \\ \vdots \\ -\frac{\nu_N}{c_N} \end{matrix} \\ \begin{matrix} 0 & \dots & \dots & \dots \end{matrix} & 0 \end{bmatrix}, \tag{13}$$

where $diag_{N-1}$ denotes a $(N-1)\times(N-1)$ dimensional diagonal matrix with index $i = 1, \dots, N-1$. Hence, the eigenvalues λ_k follow from the characteristic equation

$$0 = det\left(\frac{\partial \mathbf{q}}{\partial \mathbf{c}} - \lambda_k \mathbf{I}_{N-1}\right) \tag{14}$$

$$= det\left(-\frac{\partial \mathbf{f}}{\partial \mathbf{c}} - \lambda_k \frac{\partial \mathbf{f}}{\partial \mathbf{q}}\right) \tag{15}$$

$$= det\left(\begin{bmatrix} diag_{N-1}\left(\frac{\nu_i}{c_i} - \lambda_k \frac{\nu_i}{q_i}\right) & \begin{matrix} -\frac{\nu_N}{c_N} + \lambda_k \frac{\nu_N}{q_N} \\ \vdots \\ -\frac{\nu_N}{c_N} + \lambda_k \frac{\nu_N}{q_N} \end{matrix} \\ \begin{matrix} -\lambda_k\xi_1 & -\lambda_k\xi_2 & \dots & -\lambda_k\xi_{N-1} \end{matrix} & -\lambda_k\xi_N \end{bmatrix}\right) \tag{16}$$

For $\lambda_k \neq \frac{q_i}{c_i}$, the characteristic equation yields

$$0 = \left(\prod_{j=1}^{N-1} \frac{\nu_j}{c_j} - \lambda_k \frac{\nu_j}{q_j}\right)\left(-\lambda_k\xi_N - \sum_{i=1}^{N-1} -\frac{\lambda_k \xi_i}{\frac{\nu_i}{c_i} - \lambda_k \frac{\nu_i}{q_i}}\left(-\frac{\nu_N}{c_N} + \lambda_k \frac{\nu_N}{q_N}\right)\right) \tag{17}$$

or equivalently

$$0 = \lambda_k \sum_{i=1}^{N} \frac{\xi_i}{\frac{\nu_i}{c_i} - \lambda_k \frac{\nu_i}{q_i}}, \tag{18}$$

which has N non-negative and distinct roots

$$\frac{q_1}{c_1} > \lambda_1 > \frac{q_2}{c_2} > ... > \frac{q_k}{c_k} > \lambda_k > \frac{q_{k+1}}{c_{k+1}} > ... > \frac{q_{N-1}}{c_{N-1}} > \lambda_{N-1} > \frac{q_N}{c_N} > \lambda_N = 0. \tag{19}$$

In (19), the components are ordered in decreasing affinity to the solid phase. Note, the selectivity order in (19) is valid only until the occurrence of a so-called reversal, which is discussed next.

For $\lambda_k = \frac{q_i}{c_i}$, we find from Eq. (16) in view of the ordering introduced in Eq. (19) that λ_k also has to be equal to $\frac{q_{i+1}}{c_{i+1}}$ corresponding to a selectivity reversal $\frac{q_i}{c_i} = \frac{q_{i+1}}{c_{i+1}}$ for any $i = 1, ...N-1$. The existence and topology of such selectivity reversals in stoichiometric ion exchange with constant solution normality was studied intensively in [6, 1, 8]. In this paper results will be extended to variable solution normality and/ or ion exchange with steric hindrance. In particular it is shown that changes in the modified solution normality may also introduce selectivity reversals.

Along the selectivity reversal, the characteristic velocity is constant according to

$$\lambda_k = \frac{q_k}{c_k} = \frac{q_{k+1}}{c_{k+1}} = K_{k,k+1}^{\frac{1}{\nu_k - \nu_{k+1}}}, \tag{20}$$

corresponding to a contact discontinuity. From (20) it is clear that $\nu_k \neq \nu_{k+1}$ is a necessary condition for the existence of a selectivity reversal.

Another contact discontinuity occurs along the Nth characteristic field corresponding to $\lambda_N = 0$, i.e. $\sigma_N = 1$. According to the discussion in the previous section regarding (7), we find that the modified solution normality will only change along the Nth characteristic field but stays constant along the others. Changes of the modified solution normality propagate with the normalized interstitial velocity of one prior to all other transitions. In contrast, concentrations $c_1, \ldots, c_N$ can change along each characteristic field.

The image of the smooth transitions in the concentration phase space for fluid phase concentrations c_i is given by the corresponding eigenvectors $\mathbf{r}_k$. For $\lambda_k \neq \frac{q_k}{c_k}$ the eigenvectors follow from

$$\begin{aligned} 0 &= \left(\frac{\nu_i}{c_i} - \lambda_k \frac{\nu_i}{q_i}\right) r_{k,i} + \left(-\frac{\nu_N}{c_N} + \lambda_k \frac{\nu_N}{q_N}\right) r_{k,N}, \\ 0 &= -\lambda_k \sum_{i=1}^{N} \xi_i r_{k,i}. \end{aligned} \tag{21}$$

Recalling the characteristic equations (15), Eq. (21) is readily satisfied for

$$\mathbf{r}_k = \left[\frac{1}{\frac{\nu_1}{c_1} - \lambda_k \frac{\nu_1}{q_1}}, \ldots\ldots, \frac{1}{\frac{\nu_N}{c_N} - \lambda_k \frac{\nu_N}{q_N}}\right]^T. \tag{22}$$

Using the characteristic equation (18) for λ_k, equilibrium formulation (5) and (22) for $\mathbf{r}_k$, it can be proven that the characteristic velocity σ_k along the k-th characteristic is monotonically increasing for $\lambda_k \neq \frac{q_k}{c_k}$ and $k < N$ because of the genuine non-linearity [26]

$$\nabla \lambda_k \mathbf{r}_k < 0. \tag{23}$$

Details can be found in Appendix A.

A transition with increasing σ_k (decreasing λ_k) corresponds to a spreading wave. Transitions in the opposite direction correspond to shock waves. The shock velocity s^k follows from the integral material balances across the shock also known as the Rankine Hugoniot conditions, which are in similar form to Eq. (10)

$$s^k = \frac{1}{1 + F\frac{\Delta q_i}{\Delta c_i}}, \quad \forall i = 1, \ldots, N. \tag{24}$$

These equations also define the image of the shock waves in the concentration phase space. If $\nu_i \neq \nu_j$ for some $i \neq j$ the image of the shock waves in the concentration phase space is curved and tangent at the beginning to the integral

curves, which are defined by the eigenvectors $\mathbf{r}_k$ [25]. For $\lambda_k = \frac{q_k}{c_k} = const.$, $k < N$ or $k = N$ we find

$$\nabla \lambda_k \mathbf{r}_k = 0 \tag{25}$$

corresponding to a contact discontinuity. According to (20) $\lambda_k = \frac{q_k}{c_k}$ corresponds to a selectivity reversal. Based on Eq. (21), the related eigenvector is

$$\mathbf{r}_k = \left[0, ..., 0, r_{k,k} = \xi_k^{-1}, r_{k,k+1} = -\xi_{k+1}^{-1}, 0, ..., 0\right]^T, \quad k < N. \tag{26}$$

This represents a straight line in the concentration phase space. Due to the tangency mentioned above, the jump conditions of the corresponding contact discontinuity are also satisfied along this line and therefore it coincides with the corresponding shock curve. Remember, all previously investigated types of transitions ($k < N$) take place on some c_{tot} hyperplane (6).

In contrast, c_{tot} changes along the remaining Nth transition. The image of the contact discontinuity of the Nth characteristic field follows from the jump conditions (24) for $s^k = u$, which results in

$$\Delta q_i / \Delta c_i = 0, \tag{27}$$

and is equivalent to

$$q_i = q_i(\mathbf{c}) = q_i(\mathbf{c}^*) = q_i^*. \tag{28}$$

Therein, $\mathbf{c}^*$ represent the states before the contact discontinuity occurs, and $\mathbf{c}$ represents the states after the contact discontinuity occurs. Since the contact discontinuity corresponding to λ_N is always traveling first in time, the state before as well as c_{tot} before and after the occurrence of the contact discontinuity follow from the given boundary and initial conditions. Depending on these quantities the state after the occurrence of the contact discontinuity can

be calculated from the jump conditions (28) and the equilibrium relations (2) according to

$$
\begin{aligned}
q_i &= c_i K_{iN}^{\frac{1}{\nu_i}} \left(\frac{q_N}{c_N}\right)^{\frac{\nu_N}{\nu_i}} = c_i^* K_{iN}^{\frac{1}{\nu_i}} \left(\frac{q_N^*}{c_N^*}\right)^{\frac{\nu_N}{\nu_i}} = q_i^*. \\
c_i \left(\frac{q_N}{c_N}\right)^{\frac{\nu_N}{\nu_i}} &= c_i^* \left(\frac{q_N}{c_N^*}\right)^{\frac{\nu_N}{\nu_i}}, \qquad (29)
\end{aligned}
$$

$$
c_i = c_i^* \left(\frac{c_N}{c_N^*}\right)^{\frac{\nu_N}{\nu_i}}. \qquad (30)
$$

The unknown variable c_N in the curves (30) for c_i depend on c_{tot}. For any given c_{tot} value, (30) reduces to a point due to the intersection with the corresponding c_{tot} hyperplane (6), which results in

$$
0 = \Phi(c_N) = \sum_{i=1}^{N} \xi_i c_i^* \left(\frac{c_N}{c_N^*}\right)^{\frac{\nu_N}{\nu_i}} - c_{tot}. \qquad (31)
$$

Thus, the remaining components c_i can be obtained from (30).

It is worth noting that the representation of the jump conditions of the contact discontinuity (28) in the concentration phase space are curved but coincide with the integral curves of the corresponding spreading wave solution, which is shown in the following. The relation between integral curves and eigenvectors corresponding to λ_N is

$$
\frac{\mathrm{d}c_i}{\mathrm{d}c_N} = \frac{r_{N,i}}{r_{N,N}} = \frac{\nu_N}{\nu_i}\frac{c_i}{c_N}. \qquad (32)
$$

Eq. (32) can be easily integrated between two states $\mathbf{c}^*$, $\mathbf{c}$ reversing the chain rule of differentiation, thus separating the variables c_i and c_N

$$
\begin{aligned}
\nu_i \int_{c_i^*}^{c_i} \frac{\mathrm{d}\tilde{c}_i}{\tilde{c}_i} &= \nu_N \int_{c_i^*}^{c_i} \frac{\mathrm{d}\tilde{c}_N}{\tilde{c}_N}, \\
\nu_i \ln\left(\frac{c_i}{c_i^*}\right) &= \nu_N \ln\left(\frac{c_N}{c_N^*}\right), \qquad (33) \\
\hookrightarrow c_i &= c_i^* \left(\frac{c_N}{c_N^*}\right)^{\frac{\nu_N}{\nu_i}},
\end{aligned}
$$

which is identical to the curves in (30).

4. Selectivity reversals

One of the most significant features of the adsorption based on the stoichiometric mass action law is the possible existence of selectivity reversals, which were first investigated in detail by Tondeur [6] and Helfferich & Klein [1] for constant solution normality and no steric hindrance. Focus in [1, 6] was on loading behavior. More recently, the role of selectivity reversals for chromatographic cycles and pulse development was discussed in [8]. Since the SMA is an extension of stoichiometric mass action law, the question arises how this extension affects the properties of the selectivity reversals. Based on the results for the equilibrium theory in Section 3, the spectral results of the SMA related to a selectivity reversal

$$\lambda_j = \frac{q_j}{c_j} = \frac{q_k}{c_k}, \tag{34}$$

are similar to the ones for the stoichiometric mass action law in [8]. In particular, the related contact discontinuity is described by a straight line parallel to the eigenvector $\mathbf{r}_j$ of the form (26), where only the two reversal participating components 'j' and 'k' change. However if steric factors p_i are non-zero, they readily affect (26) through (4). Note, the components 'j' and 'k' do not necessarily need to satisfy $|j-k| = 1$ since the possibility that another selectivity reversal has already occurred changes the initial order in (19) accordingly.

In the following, we derive a topological representation of the selectivity reversals accounting for steric effects and the variable solution normality. For this purpose, Eq. (34) is assumed to be satisfied in conjunction with Eqs. (5). Together they form a set of N equations allowing for the elimination of N variables q_i in (3). Hence, the corresponding region in the concentration phase space is represented by the 'jk' reversal hyperplane

$$0 = \sum_{i \neq j,k} \xi_i c_i \left(K_{ij} K_{jk}^{\frac{\nu_j}{\nu_j - \nu_k}} \right)^{\frac{1}{\nu_i}} + \left(\xi_j c_j + \xi_k c_k \right) K_{jk}^{\frac{1}{\nu_j - \nu_k}} - q_{tot}, \tag{35}$$

or equivalently

$$0 = \sum_{i=1}^{N} \xi_i c_i \left(K_{ij} K_{jk}^{\frac{\nu_j}{\nu_j - \nu_k}} \right)^{\frac{1}{\nu_i}} - q_{tot}, \tag{36}$$

using $K_{jj} = 1$ and $K_{kj} = K_{jk}^{-1}$. Compared to the selectivity reversal described in [1], the dimension of the reversal hyperplane is increased by one to $N - 1$, which is a direct consequence of the missing closing condition for the fluid phase concentrations due to the variability of the solution normality. Furthermore, the reversal hyperplane (35,36) depends not only on the parameters q_{tot}, K_{ij}, K_{jk} and ν_i but also on ξ_i, which can contain non-vanishing steric factors p_i.

Physically meaningful results are obtained from equation (36) if the 'jk' hyperplane intersects exclusively the edges of the positive orthant, i.e. $c_i > 0$ for all $i = 1, \ldots, N$. In other words, these intersections define the condition of the existence of the 'jk' reversal hyperplane, and they are characterized by the fact that only a single component c_i in (36) is non-zero. This gives rise to the following criteria for the existence of a 'jk' reversal hyperplane

$$0 = \xi_i c_i \left(K_{ij} K_{jk}^{\frac{\nu_j}{\nu_j - \nu_k}} \right)^{\frac{1}{\nu_i}} - q_{tot}, \quad \forall i = 1, \ldots, N. \tag{37}$$

Since all concentrations and parameters are greater than zero, both conditions are satisfied for some $c_i > 0$ independently of all q_{tot}, K_{ij}, K_{jk} and ξ_i parameter values if and only if

$$\nu_j \neq \nu_k. \tag{38}$$

Eq. (38) represents the only necessary and sufficient condition for the existence of a reversal hyperplane.

It can be shown that reversal hyperplanes have no proper intersection but can be identical. Details regarding both properties can be found in Appendix B.

The classical selectivity reversal in [1, 7, 8] assumes a constant value for c_{tot} as well as no steric hindrance since it is based on the stoichiometric mass action law. Therefore, a classical 'jk' selectivity reversal is the intersection of the corresponding c_{tot} hyperplane (6) and the 'jk' reversal hyperplane (35,36) with $\xi_i = \frac{1}{\nu_i}$. The requirement of a constant solution normality is an additional restriction, which explains the relaxed condition (38) compared to the conditions in [1].

The generalized intersection of a 'jk' reversal hyperplane with a c_{tot} hyperplane of constant modified solution normality is best represented rewriting (6) into

$$\xi_j c_j + \xi_k c_k = c_{tot} - \sum_{i \neq k,j} \xi_i c_i, \tag{39}$$

and applying (39) to (35)

$$0 = \sum_{i \neq j,k} \xi_i c_i \left[\left(K_{ij} K_{jk}^{\frac{\nu_j}{\nu_j - \nu_k}} \right)^{\frac{1}{\nu_i}} - K_{jk}^{\frac{1}{\nu_j - \nu_k}} \right] + K_{jk}^{\frac{1}{\nu_j - \nu_k}} c_{tot} - q_{tot}. \tag{40}$$

Eq. (40) describes a $N-2$ dimensional reversal hyperplane with variables $c_i,\ i \neq \{j,k\}$ and c_{tot}. Moving along trajectories with $c_{tot} = const.$ and $c_i = const.$ for all $i \neq j,k$, the right-hand side of Eq. (39) is constant, which is equivalent to the result (26). Representation (40) describes the classical selectivity reversal in [1, 7, 8] if additionally $\xi_i = \frac{1}{\nu_i}$ holds. Another crucial difference of (40) and its representation in [1] is the absence of the normalization factor $\frac{c_{tot}}{q_{tot}}$ in the equilibrium constants, which are independent of c_{tot} and q_{tot} in the present case.

In the next section, focus is on chromatographic cycles. They were also discussed in [8] for a constant solution normality. A chromatographic cycle

consists of two phases, the loading and the regeneration. In case of Riemann conditions and a variable (modified) solution normality, both phases allow for two different c_{tot} hyperplanes (6). Only one of these two c_{tot} hyperplanes need to intersect an arbitrary 'jk' reversal hyperplane in order to admit a classical 'jk' selectivity reversal. Thus, the likelihood of the chromatographic cycle to be affected by a selectivity reversal is increased compared to cycles in [8]. Moreover, one of these two c_{tot} hyperplanes does not require to assume a specific c_{tot} value but to be only in a certain interval, which further relaxes the conditions of the chromatographic cycle to be affected by a selectivity reversal. For more details, the reader is referred to Appendix C.

In case of a variable (modified) solution normality, there is an additional possibility for the intersection of a reversal hyperplane realized through the contact discontinuity of the Nth characteristic field corresponding to $\lambda_N = 0$. Such an intersection with an arbitrary 'jk' reversal hyperplane exists if the following equation

$$\begin{aligned} 0 =& \Psi(c_N) \\ =& \sum_{i=1}^{N} \xi_i c_i^* \left(\left(\frac{c_N}{c_N^*} \right)^{\nu_N} K_{ij} K_{jk}^{\frac{\nu_j}{\nu_j - \nu_k}} \right)^{\frac{1}{\nu_i}} - q_{tot}, \end{aligned} \tag{41}$$

admits a physically meaningful solution $c_N > 0$. In (41), the state $\mathbf{c}^*$ denotes the state before the occurrence of the contact discontinuity as in (28). Again, all other components can be determined from Eq. (30). Further details can also be found in Appendix C. Eq. (41) includes the special case of the stoichiometric mass action law with $\xi_i = \frac{1}{\nu_i}$. Hence, a variable solution normality increases the potential of a chromatographic cycle to be affected by a selectivity reversal even further.

5. Application examples

In this section, the additional features of the steric mass action law compared to the stoichiometric mass action law [8] are studied through simulations of a sin-

gle chromatographic column to verify the theoretical results of previous sections. In particular, the effects of a variable solution normality and the steric factors are considered separately in the first two subsections, respectively, whereas joint effects and their relation to the first two cases are studied in a third subsection. In all cases Riemann experiments are performed for three component systems with constant initial conditions and piecewise constant boundary conditions, where two of components $c_1,\ c_2$ are target components. The third component c_3 (the 'salt') can be used to affect the adsorption behavior of the other two components, thus allowing for an additional degree of freedom in process design. For a complete picture containing effects on the loading and regeneration behavior, so called chromatographic cycles are considered. They are realized via injection of pulses with a sufficient pulse width. The basic simulations parameters applied to any application example independently of the specific set-up can be found in Tab.1. Simulation results are obtained through the approach described in [8] and its extension in [21]. Note, the set-up specific parameters in the following subsections are chosen such that all significant features can be illustrated step-by-step in a compact manner. However, for a proof of principle, an example based on experimentally derived parameters is briefly presented in Appendix E.

5.1. Effect of the variable solution normality

Specific parameters are listed in Tab.2. First, we consider a classical stoichiometric set-up without steric hindrance $p_i = 0$ and with constant solution normality $c_{tot} = 2$. The column is equilibrated with $\mathbf{c}^{init} = [0, 0, 2]^T\ \frac{mol}{m^3}$, the third component only. At time unit 0 starts the injection also of the two other components with $\mathbf{c}^{load} = [0.4, 0.6, 1.2]\ \frac{mol}{m^3}$. After 10 time units the feed changes back to $\mathbf{c}^{init} = [0, 0, 2]^T\ \frac{mol}{m^3}$ for regeneration purposes of the first two components. The values of third component is specifically chosen to guarantee a constant solution normality c_{tot}. The results consisting of two shocks $S_1,\ S_2$ and two spreading waves $R_1,\ R_2$ are presented in Fig. 1. Note, no selectivity reversal occurs.

In order to investigate the effect of the variable solution normality, a similar set-up to the previous one is considered. In this case, a variable solution normality is realized through different initial conditions. In particular, a column equilibrated with c_3 only, i.e. $\mathbf{c}^{init} = [0, 0, 0.1]^T \ \frac{mol}{m^3}$ is injected with the same feed pulse of $\mathbf{c}^{load} = [0.4, 0.6, 1.2] \ \frac{mol}{m^3}$ starting at $t = 0$ and ending at $t = 10$ as in the previous set-up, which again introduces components c_1 and c_2 into the column. After 10 time units the feed is changed to $\mathbf{c}^{reg} = [0, 0, 0.5] \ \frac{mol}{m^3}$ in order ro regenerate the bed. The relevant topology is shown in Fig. 2a. There are two c_{tot} planes of interest corresponding to the values $c_{tot} = 0.5 \ \frac{mol}{m^3}$ and $c_{tot} = 2 \ \frac{mol}{m^3}$, respectively. Note, that the latter c_{tot} value is identical to the one in Fig. 1a. There are also two reversal planes (gray), but only the intermediate one between $c_{tot} = 0.5 \ \frac{mol}{m^3}$ and $c_{tot} = 2 \ \frac{mol}{m^3}$ is relevant. Corresponding numerical results are shown in Fig. 2b but are also plotted into Fig. 2a (black dashed line) showing that only the two c_{tot} planes and the two eigenvectors corresponding to $\lambda_3 = 0$ are relevant.

Considering the two contact discontinuities CD_1, CD_2 regarding $\lambda_N = 0$, their prediction based on the equilibrium theory (green) in Fig. 2a obviously match the numerical results very well. These two transitions are also highlighted in Fig. 2b. As mentioned in Section 3, c_{tot} changes only along those contact discontinuities allowing for a second relevant c_{tot} plane with $c_{tot} = 0.5 \ \frac{mol}{m^3}$ besides the one with $c_{tot} = 2 \ \frac{mol}{m^3}$. This is clearly visible in Fig. 2. For the same reason they are not present in Fig.1 with $c_{tot} = const. = 2 \ \frac{mol}{m^3}$. Note, the initial loading of the column corresponds to a $c_{tot} = 0.1 \ \frac{mol}{m^3}$ plane. As already explained in Section 3, only c_3 changes along the first contact discontinuity CD_1 with the trivial intersection $[0, 0, 2] \ \frac{mol}{m^3}$, which coincides with the initial condition in Fig. 1. Hence, the $c_{tot} = 0.1 \ \frac{mol}{m^3}$ plane does not provide more insight and is neglected here. The intersection of the second contact discontinuity CD_2, however, has to be determined from (31) and (30) with $\mathbf{c}* = \mathbf{c}^{load}$ and yields $\mathbf{c} = [0.1898, 0.1350, 0.2701]^T \ \frac{mol}{m^3}$.

Investigating the remaining transitions it is sufficient to consider the projections of the two c_{tot} planes in the c_1, c_2-space. The loading behavior on the

$c_{tot} = 2\ \frac{mol}{m^3}$ plane with two shocks S_1, S_2 in Fig. 3 for the two target components c_1, c_2 is identical to the one in Fig. 1 since the c_{tot} planes and initial conditions on this plane are identical. The regeneration behavior on the $c_{tot} = 0.5\ \frac{mol}{m^3}$ plane in Fig. 4a consists also of two spreading waves R_1, R_2 but it is obviously different from the regeneration in Fig. 1a. Neither of the two c_{tot} planes Fig. 3a, Fig. 4a shows the existence of a selectivity reversal. However, in Fig. 4b component c_1 is obviously stronger adsorbing in the regeneration phase, whereas in Fig. 1b the second component c_2 is stronger adsorbing during the regeneration of c_1 and c_2. This selectivity reversal can be easily explained by means of Fig. 2a. It shows that the contact discontinuity CD_2 crosses the '1, 2' reversal plane, which explains the reversed regeneration behavior on the $c_{tot} = 2\ \frac{mol}{m^3}$ plane in Fig. 1 and on the $c_{tot} = 0.5\ \frac{mol}{m^3}$ plane in Fig. 4. The intersection can be calculated from (41), (30) and yields $\mathbf{c}^R = [0.2829, 0.3001, 0.6002]^T\ \frac{mol}{m^3}$. Since this contact discontinuity admits a change in c_{tot}, this variability in c_{tot} based on different initial conditions is directly connected to the presence of the '1, 2' selectivity reversal in the chromatographic cycle. Again, the two shocks highlighted in Fig. 3b and two spreading waves highlighted in Fig. 4b are also plotted (black dashed lines) into the respective c_1, c_2-space Fig. 3a, 4a, and they are readily predicted by the equilibrium theory (green lines).

A comparison of Fig. 3a and Fig. 4a shows that the monotonicity of the eigenvalues on the red integral curves reversed but the watershed changed also its position significantly from the c_1-axis to the c_2-axis. Hence, a variable solution normality allows in general for significant topological changes of the path grid on the c_{tot} hyperplanes.

The reversal zones introduced in Appendix C yield for this specific example $[c^l_{tot}, c^u_{tot}]_{1,2} = \frac{1}{9}[6, 16]\ \frac{mol}{m^3}$ and $[c^l_{tot}, c^u_{tot}]_{1,3} = \frac{1}{32}[3, 8]\ \frac{mol}{m^3}$. For the relevant '1, 2' reversal plane and the two cycle participating c_{tot} planes holds $\bar{c}_{tot} = \frac{1}{9}[4.5, 18]$ and therefore $[c^l_{tot}, c^u_{tot}]_{1,2} \subset \bar{c}_{tot}$, which by itself guarantees the '1, 2' selectivity reversal to occur during the chromatographic cycle without further knowledge.

5.2. Effect of the steric factors

Parameters required for the examples in this section are listed in Tab.2 and 3. In order to avoid any confusion with the effect of the variable solution normality, the following set-ups are designed such that $c_{tot}^{I} = c_{tot}^{II} = c_{tot} = const = 0.5\ \frac{mol}{m^3}$ for a classical stoichiometric-based mass action law 'I' and a steric-based mass action law 'II'. Thus, only the effect of the steric factors is considered, and it also allows to consider the relevant projections into the c_1,c_2-space for a simpler presentation.

Fig. 5 allows for an efficient comparison. Their quantitative difference is apparent, but also their qualitative similarity can be conjectured, which is consistent with the results in Appendix D. Therein, a bijective coordinate transformation is shown to exist between adsorption models differing only in their steric factors if they are subject to an identical (modified) solution normality as in the present case with $c_{tot} = const = 0.5\ \frac{mol}{m^3}$.

In order to quantify this similarity, a chromatographic cycle on the stoichiometric c_{tot} plane (Fig. 6) is compared with a chromatographic cycle having corresponding scaled initial and boundary conditions (Fig. 6) subject to (D.1). In the stoichiometric case, the column is equilibrated with $\mathbf{c}^{init} = [0, 0, 0.5]^T\ \frac{mol}{m^3}$. A pulse feed is injected at time unit 0 with $\mathbf{c}^{I,load} = [0.3, 0.3, 0.05]^T\ \frac{mol}{m^3}$ and changed back to $\mathbf{c}^{regen} = [0, 0, 0.5]^T\ \frac{mol}{m^3}$ at 10 time units. In the steric case, the column is also equilibrated with $\mathbf{c}^{init} = [0, 0, 0.5]^T\ \frac{mol}{m^3}$. Similarly, a pulse feed is injected at $t = 0$ with $\mathbf{c}^{II,load} = [0.06, 0.15, 0.05]^T\ \frac{mol}{m^3}$ and changed back to $\mathbf{c}^{regen} = [0, 0, 0.5]^T\ \frac{mol}{m^3}$ at $t = 10$. Comparing the profiles in Fig. 6b and Fig. 7b, the quantitative difference is again evident as is their qualitative similarity. Both showing two shocks S_1, S_2 and two spreading waves R_1, R_2 in the same order at identical time units. Moreover, the selectivity of the components is identical. Applying the transformation (D.1) to the steric solution in 7b results in concentration profiles identical to the stoichiometric ones in 6b. Hence, the information of the stoichiometric and steric c_{tot} plane are redundant. As shown in Appendix D, the complete concentration phase space are redundant for both cases.

The demonstrated example is representative for the general effect of steric factors on all results derived in previous sections. Steric factors can have a significant quantitative impact but do not affect any result qualitatively.

5.3. Joint effects of steric factors and variable solution normality

The additionally required parameters related to this subsection are listed in Tab.2 and 3. The following set-up considers again two c_{tot} planes with different values $c_{tot}^I \neq c_{tot}^{II}$. Similar to the previous subsection, the classical stoichiometric case is considered ($\xi_i^I = \frac{1}{\nu_i}$) as well as a steric case ($xi_i^{II} = \frac{1}{\nu_i} + p_i$) with the same change of steric factors from $\mathbf{p}^I = [0,0,0]^T$ to $\mathbf{p}^{II} = [2,1,0]^T$, while all other parameters are again identical. However, instead of scaling the boundary and initial condition to keep the solution normality c_{tot}^I and modified solution normality c_{tot}^{II} on both planes identical, the feed is kept constant $c^{I,load} = c^{II,load} = c^{load}$. This set-up reflects the situation of changing one or more components with different steric factors while keeping all other experimental conditions identical.

The stoichiometric case without steric hindrance and $c_{tot}^I = 0.5\ \frac{mol}{m^3}$ and the case with steric hindrance and $c_{tot}^{II} = 1.2\ \frac{mol}{m^3}$ are considered. Due to the definition of the set-up with an identical feed $\mathbf{c}^{load}$, their intersection includes the point $\mathbf{c}^{load} = [0.2, 0.3, 0.1]^T\ \frac{mol}{m^3}$. As before steric factors effect positioning and orientation in the concentration phase space. Since their c_{tot} values are different, the transformation (D.1) does not exist. However, both c_{tot} are constant realized through an specific choice of c_3 values, which again allows for a simplified and effective comparison in the c_1, c_2-space in the remainder.

In the stoichiometric case, the column is equilibrated with $\mathbf{c}^{I,init} = [0,0,0.5]^T\ \frac{mol}{m^3}$. A pulse that introduces components c_1 and c_2 starts with $\mathbf{c}^{load} = [0.2, 0.3, 0.1]^T\ \frac{mol}{m^3}$ at $t = 0$ and changes back to $\mathbf{c}^{I,regen} = [0,0,0.5]^T\ \frac{mol}{m^3}$ at $t = 10$ for the regeneration of the first two components. The third component is changed such that $c_{tot} = 0.5\ \frac{mol}{m^3}$ is kept constant. The c_{tot}^I plane including the validation of numerical results (black dashed line) with equilibrium theory prediction (green and orange) as well as the numerically obtained profiles are shown in Fig. 8.

These results can be compared with the corresponding ones on the c_{tot}^{II} plane in Fig. 9. A similar pulse set-up was performed here starting with an equilibrated column $\mathbf{c}^{II,init} = [0, 0, 1.2]^T \ \frac{mol}{m^3}$ and a pulse at time unit 0 with the same $\mathbf{c}^{load} = [0.2, 0.3, 0.1]^T \ \frac{mol}{m^3}$ that is changed back at 10 time units to $\mathbf{c}^{II,regen} = [0, 0, 1.2]^T \ \frac{mol}{m^3}$. The different ξ_i^{II} values in this case lead to the different $c_{tot}^{II} = 1.2 \ \frac{mol}{m^3}$ and the corresponding adjustment of the third component to keep it constant, i.e. different initial and regeneration conditions. Again, numerical results and equilibrium theory prediction are in excellent agreement.

Comparing Fig. 8a and Fig. 9a, apart from the fact that both show two shocks S_1, S_2 during the loading and two spreading waves R_1, R_2 during the regeneration, two apparent distinction can be seen. First, only in Fig. 9a a selectivity reversal (gray) can be observed. Second, the chromatographic cycles are reversed in the sense that in Fig. 8, component c_1 is stronger adsorbing during the loading phase of the pulse, whereas in Fig. 9 component c_2 is stronger adsorbing in the same phase. A similar situation occurs if we operated on the c_{tot}^{II} plane in Fig. 9a with a $\mathbf{c}^{load}$ on different sites of the selectivity reversal, which has been presented in [8].

For both adoption models 'I' and 'II', the fixed $\mathbf{c}^{load}$ introduces a difference in c_{tot} values due to different steric factors. This results in significant topological differences between the two c_{tot} planes in Fig. 8a and Fig. 9a that can be predicted by the equilibrium theory only if applied to case 'I' and 'II' separately.

In the present case, we consider two chromatographic cycles separately. However, using the results from the preceding subsection, the concentration phase space corresponding to 'II' contains a $\tilde{c}_{tot}$ plane that is similar to the c_{tot}^{I} plane in Fig. 8a in the sense of (D.1). If also $\mathbf{c}^{II,regen} = \mathbf{c}^{I,regen}$ holds, the chromatographic cycle for 'II' will consist of the two relevant $\tilde{c}_{tot}$ and c_{tot}^{II} planes, which are connected by a contact discontinuity corresponding to $\lambda_3 = 0$. Thus, two significantly different c_{tot} planes are present in a single chromatic cycle, which is then similar to the result in Subsection 5.1 with constant steric factors. In particular, if the inverse mapping of (D.1) is applied to the solution in Fig. 2, a similar result with the same qualitative behavior in the concentrations phase

space of 'II' is obtained. Consequently, also in case of a variable solution normality, the effect of steric factors is quantitative only, which is consistent with the results in Appendix D.

Since it is a straight forward extension of the results in the previous subsection and does not yield any additional insight, the corresponding simulations in a three dimensional concentration state space are omitted.

6. Conclusions

Equilibrium theory for ion exchange chromatography was extended to account for variable solution normality and steric hindrance. Possible fields of application are separation of proteins where often salt gradients are applied and also amino acids [27, 28]. Important findings are: that variable solution normality may introduce selectivity reversals and may thereby change the solution qualitatively (order of elution, types of transitions etc.). It was proven that in contrast to this, steric hindrance affects the solution only quantitatively (plateau values, propagation velocities etc.). The paper provides methods and tools for the prediction of column dynamics and therefore builds an important basis for future work on conceptional design and control of single- and multi-column systems. Limitations for protein separations are due to the limitations of the SMA isotherm used in this paper. In particular, the assumption of a constant pH. For Systems with variable pH additional effects may arise, which are not covered by the present theory. For such systems, at the moment only a numerical approach is possible [15].

Acknowledgments.

The financial support of the International Max Planck Research School for Advanced Methods in Process and Systems Engineering - IMPRS ProEng is greatly acknowledged. The research was also supported by the center of dynamic systems (CDS), funded by the EU-programme ERDF (European Regional Development Fund).

Notation

c_i	fluid phase concentration of component i	$[\frac{mol}{m^3}]$
c_{tot}	modified solution normality	$[\frac{mol}{m^3}]$
ϵ	void fraction	$[-]$
F	phase ratio	$[-]$
K_{iN}	equilibrium constant of component i and N	$[-]$
L	length of column	$[m]$
λ_k	k-th eigenvalue	$[-]$
N	number of components	$[-]$
N_z	number of spatial grid points	$[-]$
μ_i	characteristic charge of component i	$[-]$
ν_i	stoichiometric coefficient of component i	$[-]$
p_i	steric factor of component i	$[-]$
q_i	solid phase concentration of component i	$[\frac{mol}{m^3}]$
q_{tot}	exchanger capacity	$[\frac{mol}{m^3}]$
$r_{k,i}$	i-th entry of k-th eigenvector	$[\frac{mol}{m^3}]$
s^k	k-th shock velocity	$[\frac{m}{s}]$
σ_k	k-th characteristic velocity	$[\frac{m}{s}]$
t	normalized time coordinate	$[-]$
t^*	time coordinate	$[s]$
u	interstitial velocity	$[\frac{m}{s}]$
ξ_i	generalized ion exchange factor of component i	$[-]$
z	normalized space coordinate	$[-]$
z^*	space coordinate	$[m]$

References

[1] F. G. Helfferich, G. Klein, Multicomponent Chromatography. Theory of Interference, M. Dekker, New York, 1970.

[2] H.-K. Rhee, R. Aris, N. R. Amundson, First-Order Partial Differential Equations: Volume II – Theory and Application of Hyperbolic Systems of Quasilinear Equations, Prentice Hall, New Jersey, 1989.

[3] G. Guiochon, S. Golshan-Shirazi, A. Katti, Fundamentals of Preparative and Nonlinear Chromatography, Academic Press, Boston, 1994.

[4] M. Mazzotti, A. Rajendran, Equilibrium theory-based analysis of nonlinear waves in separation processes, Annual Review of Chemical and Biomolecular Engineering 4 (2013) 119–141.

[5] F. Steinebach, M. Krättli, G. Storti, M. Morbidelli, Equilibrium theory based design space for the multicolumn countercurrent solvent gradient purification process, I& EC research 56 (2017) 13482–13489.

[6] D. Tondeur, Theorie des colonnes d'change d'ions, ph.D. Thesis, Universite de Nancy (1969).

[7] D. Tondeur, Theory of ion-exchnage columns, Chemical Engineering Journal 1 (1970) 337–346.

[8] M. Fechtner, A. Kienle, Efficient simulation and equilibrium theory for adsorption processes with implicit adsorption isotherms – mass action equilibria, Chemical Engineering Science 171 (2017) 471–480. doi:10.1016/j.ces.2017.06.004.

[9] S. Gallant, A. Kundu, S. Cramer, Modeling non-linear elution of proteins in ion-exchange chromatography, Journal of Chromatography A 702 (1995) 125–142.

[10] V. Natarajan, S. Cramer, Comparison of linear gradient and displacement separations in ion-exchange systems, Biotechnology and Bioengineering 78.

[11] H. Karkov, L. Sejergaard, S. Cramer, Methods development in multimodal chromatography with mobilephase modifiers using the steric mass action model, Journal of Chromatography A 1318 (2013) 149–155.

[12] G. Carta, A. Jungbauer, Protein Chromatography, Vol. 1, WILEY-VCH Verlag GmbH & Co. KGaA, Weinheim, 2010.

[13] J. Janson, Protein Purification, Vol. 1, JOHN WILEY & SONS. INC., New Jersey, 2011.

[14] C. Brooks, S. Cramer, Steric mass-action ion exchange: Displacement profiles and induced salt gradients, AIChE Journal 38(12) (1992) 1969–1978.

[15] T. Pabst, G. Carta, Separation of protein charge variants with induced ph gradients using anion exchange chromatographic columns, Biotechnol. Prog. 24 (2008) 1096–1106.

[16] T. Pabst, G. Carta, ph transitions in cation exchange chromatographic columns containing weak acid groups, J. Chrom. A 1142 (2007) 19–31.

[17] S. Gallant, S. Vunnum, S. Cramer, Modeling gradient elution of proteins in ion-exchange chromatography, AIChE Journal 42.

[18] D. Frey, Local-equilibrium behavior of retained ph and ionic strength gradients in preparative chromatography, Biotechnol. Prog. 12 (1996) 65–72.

[19] J. Pérez, D. Frey, Local-equilibrium behavior of retained ph and ionic strength gradients in preparative chromatography, Biotechnol. Prog. 21 (2005) 902–910.

[20] A. Velayudhan, C. Horváth, Preparative chromatography of proteins analysis of the multivalent ion-exchange formalism, J. Chrom. 443 (1988) 13–29.

[21] M. Fechtner, M. Kaspereit, A. Kienle, Efficient simulation of ion exchange chromatography with application to bioseparations, Computer Aided Chem. Eng. 43 (2018) 295–300. doi:10.1016/B978-0-444-64235-6.50055-3.

[22] W. E. Schiesser, The Numerical Method of Lines Integration of Partial Differential Equations, Academic Press, San Diego, 1991.

[23] MATLAB, version 8.4.0 (R2014b), The MathWorks Inc., Natick, Massachusetts, 2014.

[24] J. Unger, A. Kröner, W. Marquardt, Structural analysis of differential-algebraic equation systems: Theory and applications, Computers & Chemical Engineering 19 (1995) 867–882.

[25] J. Smoller, Shock Waves and Reaction–Diffusion Equations, 2nd Edition, Springer, New York, 1994.

[26] P. Lax, Hyperbolic Systems of Conservation Laws and the Mathematical Theory of Shock Waves, Vol. 1, CBMS-NSF Regional Conference Series in Applied Mathematics, 1973.

[27] H. Nagai, G. Carta, Lysine adsorption on cation exchange resin. i. ion exchange equilibrium and kinetics, Sep. Sci. Technol. 39.

[28] H. Nagai, G. Carta, Lysine adsorption on cation exchange resin. ii. column adsorption/desorption behavior and modeling, Sep. Sci. Technol. 39.

[29] S. Gallant, S. Vunnum, S. Cramer, Optimization of preparative ion-exchange chromatography of proteins: linear gradient separations, Journal of Chromatography A 725 (1996) 295–314.

Appendix A. Genuine non-linearity

The following considerations exclude $\lambda_k = 0$ and $\lambda_k = \frac{q_k}{c_k}$ for any k. Both cases are shown to be linear degenerate in Section 3. In the remainder we show that the k-th field is genuinely non-linear for a certain subset $\mathcal{C}$ of $\mathbb{R}^N_+$ according to

$$\nabla\lambda_k(\mathbf{c})\mathbf{r}_k(\mathbf{c}) \neq 0, \ \forall \mathbf{c} \in \mathcal{C}, \tag{A.1}$$

holds. The gradient of λ_k can be obtained through implicit differentiation of

$$\alpha(\mathbf{c}, \mathbf{q}, \lambda_k) = 0 = \lambda_k \sum_{i=1}^{N} \frac{\frac{\xi_i}{\nu_i}}{\frac{1}{c_i} - \lambda_k \frac{1}{q_i}}, \tag{A.2}$$

which results in

$$\frac{\partial \lambda_k}{\partial c_j} = -\left(\frac{\partial \alpha}{\partial \lambda_k}\right)^{-1}_{\mathbf{c},\mathbf{q}} \left(\left(\frac{\partial \alpha}{\partial c_j}\right)_{\mathbf{c}\setminus c_j,\mathbf{q},\lambda_k} + \sum_{l=1} \left(\frac{\partial \alpha}{\partial q_l}\right)_{\mathbf{c},\mathbf{q}\setminus q_l,\lambda_k} \frac{\partial q_l}{\partial c_j} \right). \tag{A.3}$$

Hereafter, constant held variables will be omitted for clarity of presentation. Results for the derivatives in (A.3) are summarized in the following

$$\begin{aligned}
\frac{\partial \alpha}{\partial \lambda_k} &= \lambda_k \sum_{i=1}^{N} \frac{\frac{\xi_i}{\nu_i}\frac{1}{q_i}}{\left(\frac{1}{c_i} - \lambda_k \frac{1}{q_i}\right)^2}, \\
\frac{\partial \alpha}{\partial c_j} &= \frac{\lambda_k}{c_j^2} \frac{\frac{\xi_j}{\nu_j}}{\left(\frac{1}{c_j} - \lambda_k \frac{1}{q_j}\right)^2}, \\
\frac{\partial \alpha}{\partial q_l} &= -\frac{\lambda_k^2}{q_l^2} \frac{\frac{\xi_l}{\nu_l}}{\left(\frac{1}{c_l} - \lambda_k \frac{1}{q_l}\right)^2}, \\
\frac{\partial q_l}{\partial c_j} &= \frac{\nu_N}{\nu_l}\frac{q_l}{q_N}\left(\frac{\partial q_N}{\partial c_j} - \frac{q_N}{c_N}\delta_{jN}\right) + \frac{q_j}{c_j}\delta_{jl}, \\
&\forall k, j, l.
\end{aligned} \tag{A.4}$$

Here, δ denotes the Kronecker delta. The last equation in (A.4) contains $\frac{\partial q_N}{\partial c_j}$, which can also be obtained through implicit differentiation of

$$\beta(\mathbf{c}, q_N) = 0 = q_{tot} - \sum_{m=1}^{N} \xi_m c_m K_{mN}^{\frac{1}{\nu_m}} \left(\frac{q_N}{c_N}\right)^{\frac{\nu_N}{\nu_m}}, \tag{A.5}$$

resulting in

$$\begin{aligned} \frac{\partial q_N}{\partial c_j} &= -\left(\frac{\partial \beta}{\partial q_N}\right)_{\mathbf{c}}^{-1} \left(\frac{\partial \beta}{\partial c_j}\right)_{\mathbf{c}\setminus c_j, q_N}, \\ &= -\frac{q_N}{\nu_N} \left(\sum_{m=1}^{N} \frac{\xi_m}{\nu_m} q_m\right)^{-1} \xi_j \frac{q_j}{c_j} + \frac{q_N}{c_N} \delta_{jN}, \end{aligned} \tag{A.6}$$

which allows us to write

$$\frac{\partial q_l}{\partial c_j} = -\frac{q_l}{\nu_l} \left(\sum_{m=1}^{N} \frac{\xi_m}{\nu_m} q_m\right)^{-1} \xi_j \frac{q_j}{c_j} + \frac{q_j}{c_j} \delta_{jl}. \tag{A.7}$$

Therefore, an element of the gradient of any λ_k can be written as follows

$$\begin{aligned} &\frac{\partial \lambda_k}{\partial c_j} = -P(Q_j + R_j) \\ &P = \left(\sum_{i=1}^{N} \frac{\frac{\xi_i}{\nu_i}\frac{1}{q_i}}{\left(\frac{1}{c_i} - \lambda_k \frac{1}{q_i}\right)^2}\right)^{-1} > 0 \\ &Q_j = \frac{\frac{\xi_j}{\nu_j}\frac{1}{c_j}}{\left(\frac{1}{c_j} - \lambda_k \frac{1}{q_j}\right)} \\ &R_j = \lambda_k \sum_{l=1}^{N} \frac{\frac{\xi_l}{\nu_l^2}\frac{1}{q_l}}{\left(\frac{1}{c_l} - \lambda_k \frac{1}{q_l}\right)^2} \left(\sum_{m=1}^{N} \frac{\xi_m}{\nu_m} q_m\right)^{-1} \xi_j \frac{q_j}{c_j} = R\, \xi_j \frac{q_j}{c_j} > 0 \\ &\forall k, j. \end{aligned} \tag{A.8}$$

Having now a complete description of $\nabla \lambda_k$ and the definition of the corresponding non-trivial eigenvector $\mathbf{r}_k$ in (22), the following expression is obtained

$$
\begin{aligned}
&\nabla\lambda_k(\mathbf{c})\mathbf{r}_k(\mathbf{c}) = -P(Q+RS) < 0,\\
&Q = \sum_{j=1}^{N} \frac{Q_j^2}{\frac{\xi_j}{c_j}} > 0,\\
&S = \sum_{j=1}^{N} \frac{q_j}{c_j} \frac{\frac{\xi_j}{\nu_j}}{\frac{1}{c_j} - \lambda_k \frac{1}{q_j}} > 0.
\end{aligned}
\tag{A.9}
$$

Since all parameters, concentrations and eigenvalues ($\lambda_N = 0$ already excluded) are greater than zero, the inequalities for $P,\ Q,\ R$ in (A.8,A.9) are obviously satisfied. The inequality for S in (A.9) is deduced from a lower bound that is derived in the following

$$
\begin{aligned}
&S = T + U,\\
&T = \sum_{j=1}^{k} \frac{q_j}{c_j} \frac{\frac{\xi_j}{\nu_j}}{\frac{1}{c_j} - \lambda_k \frac{1}{q_j}},\ \frac{q_j}{c_j} \geq \frac{q_k}{c_k} > \lambda_k,\\
&U = \sum_{j=k+1}^{N} \frac{q_j}{c_j} \frac{\frac{\xi_j}{\nu_j}}{\frac{1}{c_j} - \lambda_k \frac{1}{q_j}},\ \frac{q_j}{c_j} < \lambda_k < \frac{q_k}{c_k},\\
&T \geq \frac{q_k}{c_k} \sum_{j=1}^{k} \frac{\frac{\xi_j}{\nu_j}}{\frac{1}{c_j} - \lambda_k \frac{1}{q_j}},\\
&U > \frac{q_k}{c_k} \sum_{j=k+1}^{N} \frac{\frac{\xi_j}{\nu_j}}{\frac{1}{c_j} - \lambda_k \frac{1}{q_j}},\\
&S > \frac{q_k}{c_k} \sum_{j=1}^{N} \frac{\frac{\xi_j}{\nu_j}}{\frac{1}{c_j} - \lambda_k \frac{1}{q_j}} = 0,
\end{aligned}
\tag{A.10}
$$

where the last in equality in (A.10) can be easily deduced from (18) for positive eigenvalues. Hence, all characteristic fields of a family $k < N$ and with $\lambda_k \neq \frac{q_k}{c_k}$ are genuinely non-linear for all $\mathbf{c} \in \mathbb{R}^N_+$, i.e. no non-positive concentrations.

Appendix B. Reversal intersections

In the following it is shown that different reversal hyperplanes do not intersect each other. More precisely, the intersection of two arbitrary reversal

hyperplanes are either the hyperplanes itself or empty but no proper intersection exists. For this purpose, two arbitrary reversal hyperplanes 'jk' and 'mn' that differ in at least one of their indices are considered. From the respective representation based on (36), their intersection is defined by

$$\begin{aligned} 0 &= \sum_{i=1}^{N} \xi_i c_i \omega_i, \\ \omega_i &= \left(K_{ij} K_{jk}^{\frac{\nu_j}{\nu_j - \nu_k}} \right)^{\frac{1}{\nu_i}} - \left(K_{im} K_{mn}^{\frac{\nu_m}{\nu_m - \nu_n}} \right)^{\frac{1}{\nu_i}}. \end{aligned} \tag{B.1}$$

It can be deduced that the ω_i's have the same sign. In particular the following relations hold

$$\begin{aligned} & K_{jk}^{\frac{\nu_j}{\nu_j - \nu_k}} > K_{jm} K_{mn}^{\frac{\nu_m}{\nu_m - \nu_n}} \rightarrow \omega_i > 0, \\ & K_{jk}^{\frac{\nu_j}{\nu_j - \nu_k}} < K_{jm} K_{mn}^{\frac{\nu_m}{\nu_m - \nu_n}} \rightarrow \omega_i < 0, \\ & \forall i = 1, \ldots, N. \end{aligned} \tag{B.2}$$

In case of any given 'jk' and 'mn' reversal hyperplane, the parameters in (B.2) are fixed for all ω_i. Hence, either $\omega_i > 0$ or $\omega_i < 0$ holds. Since also all ξ_i are positive, the first equation in (B.1) requires that the c_i do not all have the same sign. In other words, it is necessary that there exists at least a single component 'l' with $c_l < 0$. Therefore, a proper intersection does not exist in the positive orthant, where $c_i > 0$ for all i.

For conditions (B.2), the intersection of two arbitrary reversal hyperplanes for physically meaningful c_i is always empty. However, if

$$\begin{aligned} & K_{jk}^{\frac{\nu_j}{\nu_j - \nu_k}} = K_{jm} K_{mn}^{\frac{\nu_m}{\nu_m - \nu_n}} \rightarrow \omega_i = 0, \\ & \forall i = 1, \ldots, N, \end{aligned} \tag{B.3}$$

we can easily conclude that both reversal hyperplanes are identical. However, the conditions in (B.3) are very specific, therefore this case is of little interest at least from a piratical point of view.

Appendix C. Reversal zones

In this section, we define an interval for c_{tot}, the so-called reversal zone, for which the corresponding c_{tot} hyperplane is guaranteed to intersect some 'jk' reversal hyperplane for physically meaningful c_i. For this purpose we consider the equation for the intersection (40) of these two types of hyperplanes and apply the same reasoning as prior to Eq. (37). Eq. (40) can be reformulated into

$$c_{tot} - q_{tot} K_{jk}^{-\frac{1}{\nu_j - \nu_k}} = \sum_{i \neq j,k} \xi_i c_i \left(K_{jk}^{\frac{1}{\nu_j - \nu_k}} - \left(K_{ij} K_{jk}^{\frac{\nu_j}{\nu_j - \nu_k}} \right)^{\frac{1}{\nu_i}} \right) K_{jk}^{-\frac{1}{\nu_j - \nu_k}}. \quad \text{(C.1)}$$

Therefore, the conditions for solutions that satisfy $c_i > 0$ yield

$$\begin{aligned} & c_{tot} - q_{tot} K_{jk}^{-\frac{1}{\nu_j - \nu_k}} = \xi_i c_i \left(K_{jk}^{\frac{1}{\nu_j - \nu_k}} - \left(K_{ij} K_{jk}^{\frac{\nu_j}{\nu_j - \nu_k}} \right)^{\frac{1}{\nu_i}} \right) K_{jk}^{-\frac{1}{\nu_j - \nu_k}}, \\ & \hookrightarrow sign\left(c_{tot} - q_{tot} K_{jk}^{-\frac{1}{\nu_j - \nu_k}} \right) = sign\left(K_{jk}^{\frac{1}{\nu_j - \nu_k}} - \left(K_{ij} K_{jk}^{\frac{\nu_j}{\nu_j - \nu_k}} \right)^{\frac{1}{\nu_i}} \right), \quad \text{(C.2)} \\ & \forall i \neq j,k. \end{aligned}$$

There are two possible cases. First,

$$\begin{aligned} & K_{jk}^{\frac{1}{\nu_j - \nu_k}} \geq \left(K_{ij} K_{jk}^{\frac{\nu_j}{\nu_j - \nu_k}} \right)^{\frac{1}{\nu_i}}, \\ & K_{jk}^{-\frac{1}{\nu_j - \nu_k}} \leq \left(K_{ij} K_{jk}^{\frac{\nu_j}{\nu_j - \nu_k}} \right)^{-\frac{1}{\nu_i}}, \quad \text{(C.3)} \\ & \forall i \neq j,k. \end{aligned}$$

Based on (C.2)

$$c_{tot} \geq q_{tot} K_{jk}^{-\frac{1}{\nu_j - \nu_k}}, \quad \text{(C.4)}$$

has to be satisfied in this case, which defines a minimum value for c_{tot}. If further

$$c_{tot} \leq q_{tot} \min_{i \neq j,k} \left[\left(K_{ij} K_{jk}^{\frac{\nu_j}{\nu_j - \nu_k}} \right)^{-\frac{1}{\nu_i}} \right], \tag{C.5}$$

holds, (C.3) is guaranteed to be satisfied due to (C.4). Thus, (C.5) defines a maximum value for c_{tot}. In this case the reversal zone in which all c_{tot} planes are guaranteed to intersect some 'jk' reversal hyperplane is

$$c_{tot} \in \left[c_{tot}^l, c_{tot}^u\right] = q_{tot} \left[K_{jk}^{-\frac{1}{\nu_j - \nu_k}}, \min_{i \neq j,k} \left[\left(K_{ij} K_{jk}^{\frac{\nu_j}{\nu_j - \nu_k}} \right)^{-\frac{1}{\nu_i}} \right] \right]. \tag{C.6}$$

In contrast to the first case, the second one assumes

$$\begin{aligned} K_{jk}^{\frac{1}{\nu_j - \nu_k}} &\leq \left(K_{ij} K_{jk}^{\frac{\nu_j}{\nu_j - \nu_k}} \right)^{\frac{1}{\nu_i}}, \\ K_{jk}^{-\frac{1}{\nu_j - \nu_k}} &\geq \left(K_{ij} K_{jk}^{\frac{\nu_j}{\nu_j - \nu_k}} \right)^{\frac{-1}{\nu_i}}, \\ &\forall i \neq j,k. \end{aligned} \tag{C.7}$$

By the same line of thought as in the first case, we readily obtain an analog reversal zone with

$$c_{tot} \in \left[c_{tot}^l, c_{tot}^u\right] = q_{tot} \left[\max_{i \neq j,k} \left[\left(K_{ij} K_{jk}^{\frac{\nu_j}{\nu_j - \nu_k}} \right)^{-\frac{1}{\nu_i}} \right], K_{jk}^{-\frac{1}{\nu_j - \nu_k}} \right]. \tag{C.8}$$

All c_{tot} hyperplanes with $c_{tot} \in [c_{tot}^l, c_{tot}^u]$ yield an intersection with the 'jk' reversal hyperplane, i.e. the classical selectivity reversal (40).

Compared to [1] where a process requires to be operated on the same c_{tot} hyperplane within the reversal zone described by (C.6) or (C.8). The chromatographic cycle with variable c_{tot} that is operated on two c_{tot} hyperplanes requires only one of them to be within the reversal zone in order to admit a classical 'jk' reversal. However, if $c_{tot} \notin [c_{tot}^l, c_{tot}^u]$ for all relevant c_{tot}, no classical selectivity reversal will be present on corresponding c_{tot} hyperplanes.

The second type of interaction with any 'jk' reversal hyperplane can be realized through its intersection with a contact discontinuity corresponding to λ_N. This transition connects c_{tot} hyperplanes over a certain range $\bar{c}_{tot} = [c^*_{tot}, c_{tot}]$, see notation in (28). There are three possible scenarios. First, if $[c^l_{tot}, c^u_{tot}] \cap \bar{c}_{tot} = \emptyset$, the Nth transition does not intersect the 'jk' reversal hyperplane for physically meaningful c_i and (41) admits definitely a solution $c_N < 0$. Second, if $[c^l_{tot}, c^u_{tot}] \cap \bar{c}_{tot} \neq \emptyset$, the contact discontinuity might intersect the 'jk' reversal hyperplane and (41) hast to be checked whether it admits $c_N > 0$ or $c_N < 0$. Finally, they definitely intersect each other in the third case if $[c^l_{tot}, c^u_{tot}] \subseteq \bar{c}_{tot}$ holds, and (41) is guaranteed to admit a solution $c_N > 0$.

Appendix D. Influence of steric hindrance

In order to understand the effect of the steric hindrance, two models are considered that differ only in their respective steric factors. Without loss of generality, we consider two cases with the adsorption equilibrium to be described by the classical stoichiometric mass action law and by the steric mass action law, respectively. In case of model 'I' $p_i = 0$ holds for all i, i.e. $\xi^I_i = \frac{1}{\nu_i}$. In contrast, model '$II$' satisfies $p_i > 0$ for at least one i. Thus, the second model accounts for the setric hindrance of at least one component with $\xi^{II}_i = \xi_i$. Note, that all other parameters (K_{iN}, ν_i and q_{tot}) of the two models are identical. These two models are investigated using two different adsorption set-ups on a single column.

In the first set-up, the feed and initial loading of the column are specifically chosen to equate the solution normality of model 'I' with the modified solution normality of model 'II', i.e. $c^I_{tot} = c^{II}_{tot} = c_{tot}$. In this case, there exists a simple linear and bijective transformation from concentration phase space II into the concentration phase space I

$$\begin{aligned} \mathbf{c}^I &= diag_N(\nu_i \xi_i)\mathbf{c}^{II} = diag_N(1 + \nu_i p_i)\mathbf{c}^{II}, \\ \mathbf{q}^I &= diag_N(\nu_i \xi_i)\mathbf{q}^{II} = diag_N(1 + \nu_i p_i)\mathbf{q}^{II}. \end{aligned} \tag{D.1}$$

Equation (D.1) can be derived from the corresponding equilibrium relation and electro neutrality condition on the exchanger of each model

$$\begin{aligned} f_i(\mathbf{q}^I, \mathbf{c}^I) &= \frac{1}{K_{iN}} \left(\frac{q_i^I}{c_i^I}\right)^{\nu_i} \left(\frac{c_N^I}{q_N^I}\right)^{\nu_N} - 1 = 0, \\ q_{tot} &= \sum_{i=1}^{N} \frac{q_i^I}{\nu_i},\ c_{tot}^I = \sum_{i=1}^{N} \frac{c_i^I}{\nu_i}, \end{aligned} \tag{D.2}$$

$$\begin{aligned} f_i(\mathbf{q}^{II}, \mathbf{c}^{II}) &= \frac{1}{K_{iN}} \left(\frac{q_i^{II}}{c_i^{II}}\right)^{\nu_i} \left(\frac{c_N^{II}}{q_N^{II}}\right)^{\nu_N} - 1 = 0, \\ q_{tot} &= \sum_{i=1}^{N} \xi_i q_i^{II},\ c_{tot}^{II} = \sum_{i=1}^{N} \xi c_i^{II}. \end{aligned} \tag{D.3}$$

Equation (D.2) can be readily transferred to Eq. (D.3) using (D.1) if and only if $c_{tot}^I = c_{tot}^{II} = c_{tot}$ holds, thus resulting in the same algebraic equations. After transformation, the Jacobian of model 'I' is identical to the one of model 'II'. Therefore, it is only necessary to obtain the concentration phase of one model since the other one can be directly constructed using (D.1).

The second set-up uses the same Riemann conditions, i.e. the same feed $\mathbf{c}_F^I = \mathbf{c}_F^{II} = \mathbf{c}_F$ and initial loading $\mathbf{c}_L^I = \mathbf{c}_L^{II} = \mathbf{c}_L$ for both models. The c_{tot}^I and c_{tot}^{II} in (D.2,D.3) have obviously different weighting factors, while the components c_i^I, c_i^{II} are subject to the initial and boundary condition. In particular, at least at the beginning of the process and once the feed conditions are established $c_i^I = c_i^{II}$ is satisfied for all i everywhere in the column. Due to the different weighting factors

$$\frac{1}{\nu_i} < \frac{1}{\nu_i} + p_i = \xi_i, \tag{D.4}$$

the corresponding solution normality and modified solution normality do not coincide in general. If indeed $c_{tot}^I \neq c_{tot}^{II}$ holds, the above simple coordinate transformation does not exist.

Note that in both set-ups the orientation and positioning of the c_{tot}^I and c_{tot}^{II} hyperplanes are different due to the different wighting factors already mentioned.

In both set-ups, for every c_{tot}^{I} hyperplane in the complete concentration phase space of 'I' there exists a similar c_{tot}^{II} hyperplane with $c_{tot}^{II} = c_{tot}^{I}$ somewhere in the concentration phase space of 'II' based on the similarity in (D.2,D.3). However, only in the in the first set-up, the boundary and initial conditions are specifically scaled for both models so that all process participating c_{tot}^{I} and c_{tot}^{II} hyperplanes are also similar in the sense of (D.1). In case of the second set-up, the process participating c_{tot}^{I} and c_{tot}^{II} hyperplanes can differ arbitrarily. Note, this difference in solution normalities is introduced due different steric factors, hence representing the case where a change in solution normality related to different steric factors affect two separate processes. The most significant differences can be the intersection with different reversal hyperplanes and different types and/ or number of watershed points.

All results presented there account for steric hindrance. Consequently, the results of the equilibrium theory as well as the results for selectivity reversals including the the ones in Appendix A, B and C are affected by steric factors. However, the effect is of a quantitative but not a qualitative nature.

Appendix E. Proof of principle

In order to give a proof of principle, the basic analogy between the academic example in Section 5 and an example based on experimentally determined SMA parameters in this Appendix is established. The specific values of the considered Riemann set-up as well as parameter values, which are taken from [29], are listed in Tab. 4. Note, we already verified our numerical approach in [21] by reproducing partially the results from [29].

In this particular case we consider only two proteins α-Chymotrypsinogen A and Cytochrome c. The strong cation-exchanger column is initially equilibrated with 30 mM sodium phosphate and the solution pH is assumed to be 6.0 at all times. At time unit 0, a buffer with 0.2 mM of both proteins and 213 mM sodium phosphate is injected for 3.114 dimensionless time units, which allows for the development of the intermediate feed plateaus. Thereafter, the feed is

changed to contain again only sodium phosphate, but still containing a high concentration of 183 mM sodium phosphate for an efficient elution of the two proteins, which especially compresses spreading wave R_1.

As a result of this Riemann experiment, a chromatographic cycle in Fig. 10 is obtained similar to the one in Fig. 2. For clarity of presentation, Fig. 10a shows only the relevant integral curves in the concentration phase space that predict the numerical solution to illustrate the validity of the equilibrium theory. The basic principles discussed in Section 5 can be immediately seen in Fig. 10b. The first contact discontinuity CD_1 only affects the sodium ion concentration. Reaching then the value of $c_{tot} = 215.1\ mM$, two shocks S_1 and S_2 follow affecting the two proteins and sodium ions but not c_{tot}. Subsequently, another contact discontinuity CD_2 follows affecting not only all components but again the value of $c_{tot} = 183\ mM$. The elution of the two proteins proceeds through two spreading waves. Again, these two transitions do not affect the value of c_{tot}. Consequently, the chromatographic cycle of this example operates on two relevant c_{tot} planes connected by CD_2, and the analogy of the present real world example to the one discussed in Section 5 can be easily established.

The same analysis can be applied here. Note, the arrows in Fig. 10a point in the direction of increasing characteristic velocity σ, therefore predicting the type of transition correctly. In case of the shocks, the integral curves are almost straight, thus nearly coinciding with the corresponding shock curves. For all other cases, the integral curves match the exact solution path in the concentration phase space. In this particular case, no selectivity reversal is present since the order of elution in Fig. 10b is preserved during the complete cycle. This can also be seen in from Fig. 10a, where the corresponding '$1, 2$' reversal plane is below all transitions that follow after CD_1. Based on this topological property it can be easily predicted that there is indeed no '$1, 2$' reversal involved between the two relevant c_{tot} values. This concludes the proof of principle.

List of Tables

parameter	value	description
$L\ [m]$	5.0	column length
$N_z\ [-]$	1000	number of grid points
$u\ [\frac{m}{s}]$	1.0	interstitial velocity
$\varepsilon\ [-]$	0.5	void fraction
$q_{tot}\ [\frac{mol}{m^3}]$	2.0	exchanger capacity
$K_{13}\ [-]$	8.0	equilibrium constant
$K_{23}\ [-]$	2.67	equilibrium constant

Table 1: Basic parameters used in all example application studies of Section 5.

parameter	value	description
ν_1 [−]	2	stoichiometric coefficient
ν_2 [−]	1	stoichiometric coefficient
ν_3 [−]	1	stoichiometric coefficient
p_1 [−]	0	steric factor
p_2 [−]	0	steric factor
p_3 [−]	0	steric factor

Table 2: Specific parameters of the stoichiometric adsorption model.

parameter	value	description
ν_1 [−]	2	stoichiometric coefficient
ν_2 [−]	1	stoichiometric coefficient
ν_3 [−]	1	stoichiometric coefficient
p_1 [−]	2	steric factor
p_2 [−]	1	steric factor
p_3 [−]	0	steric factor

Table 3: Specific parameters of the steric adsorption model.

parameter	value	description
$L\ [mm]$	54.0	column length
$N_z\ [-]$	1000	number of grid points
$u\ [\frac{mm}{s}]$	0.4244	interstitial velocity
$\varepsilon\ [-]$	0.73	void fraction
$q_{tot}\ [mM]$	525.0	exchanger capacity
$K_{31}\ [-]$	0.0135	equilibrium constant
$K_{32}\ [-]$	0.045	equilibrium constant
$\mu_1\ [-]$	5.03	characteristic charge
$\mu_2\ [-]$	5.67	characteristic charge
$\mu_3\ [-]$	1.0	characteristic charge
$p_1\ [-]$	7.43	steric factor
$p_2\ [-]$	27.4	steric factor
$p_3\ [-]$	0.0	steric factor

Table 4: Riemann specifications and experimental parameters.

List of Figures

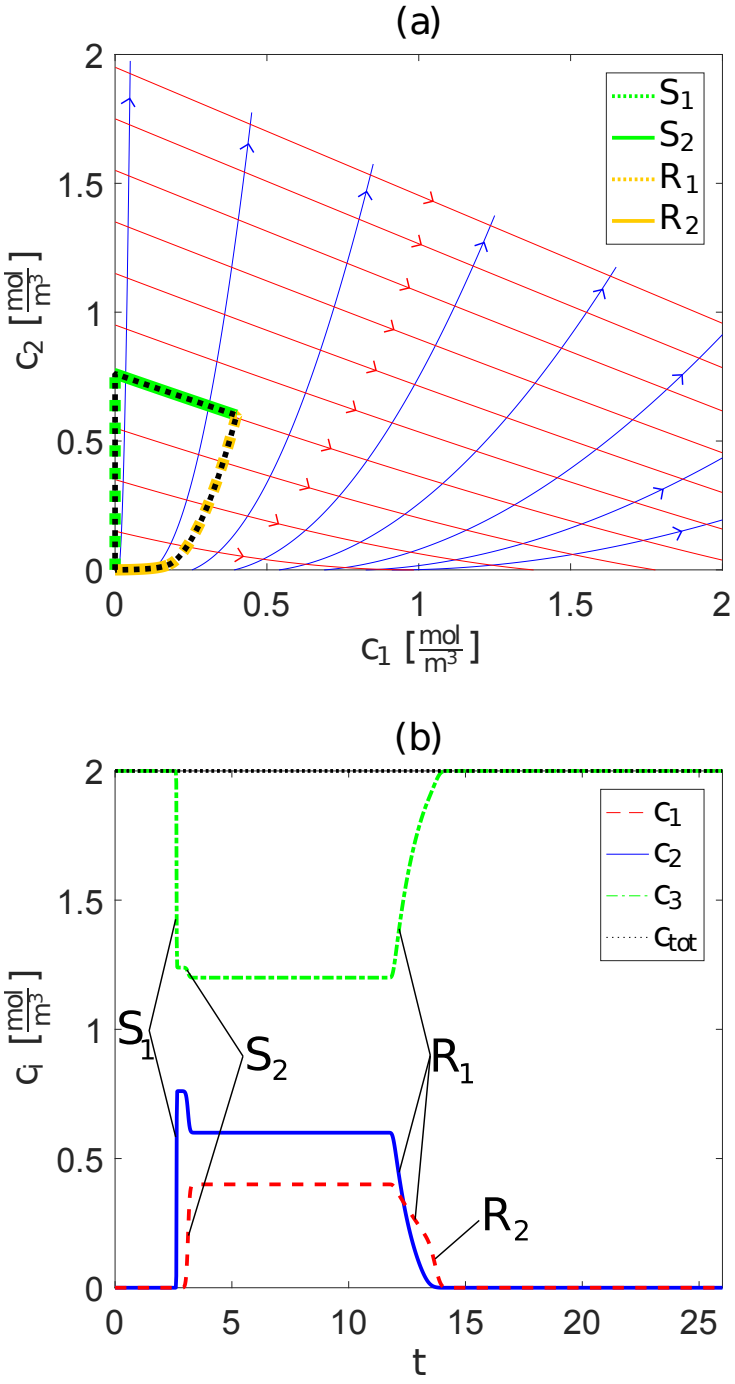

Figure 1: (a) Chromatographic cycle in the concentration phase space realized by a pulse experiment of the classical stoichiometric ion exchange with constant solution normality c_{tot}. Numerical results (black dashed line) overlap solution predicted by the equilibrium theory (green and orange lines). (b) Corresponding elution profile $c_i(z)$ indicating two shocks S_1, S_2 and two spreading waves R_1, R_2.

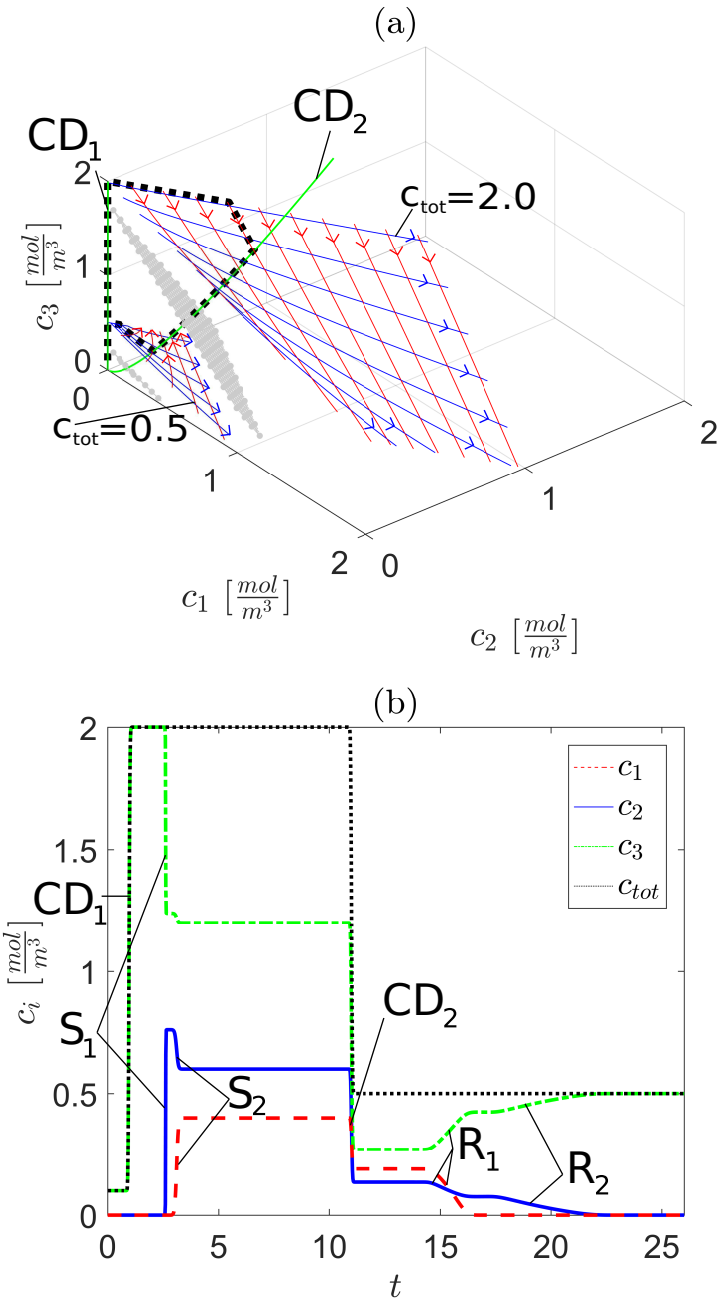

Figure 2: (a) Chromatographic cycle in the concentration phase space realized by a pulse experiment of the classical stoichiometric ion exchange with variable solution normality c_{tot}. Gray planes indicate reversal planes '1, 2' and '1, 3'. Numerical results (black dashed line) overlap two contact discontinuities CD_1, CD_2 (solid green lines) while the remaining transitions are located in two different planes $c_{tot} = 0.5\ \frac{mol}{m^3}$, $c_{tot} = 2\ \frac{mol}{m^3}$, which are all predicted by the equilibrium theory. (b) Corresponding elution profile $c_i(z)$ indicating two additional contact discontinuities CD_1, CD_2 compared to Fig. 1.

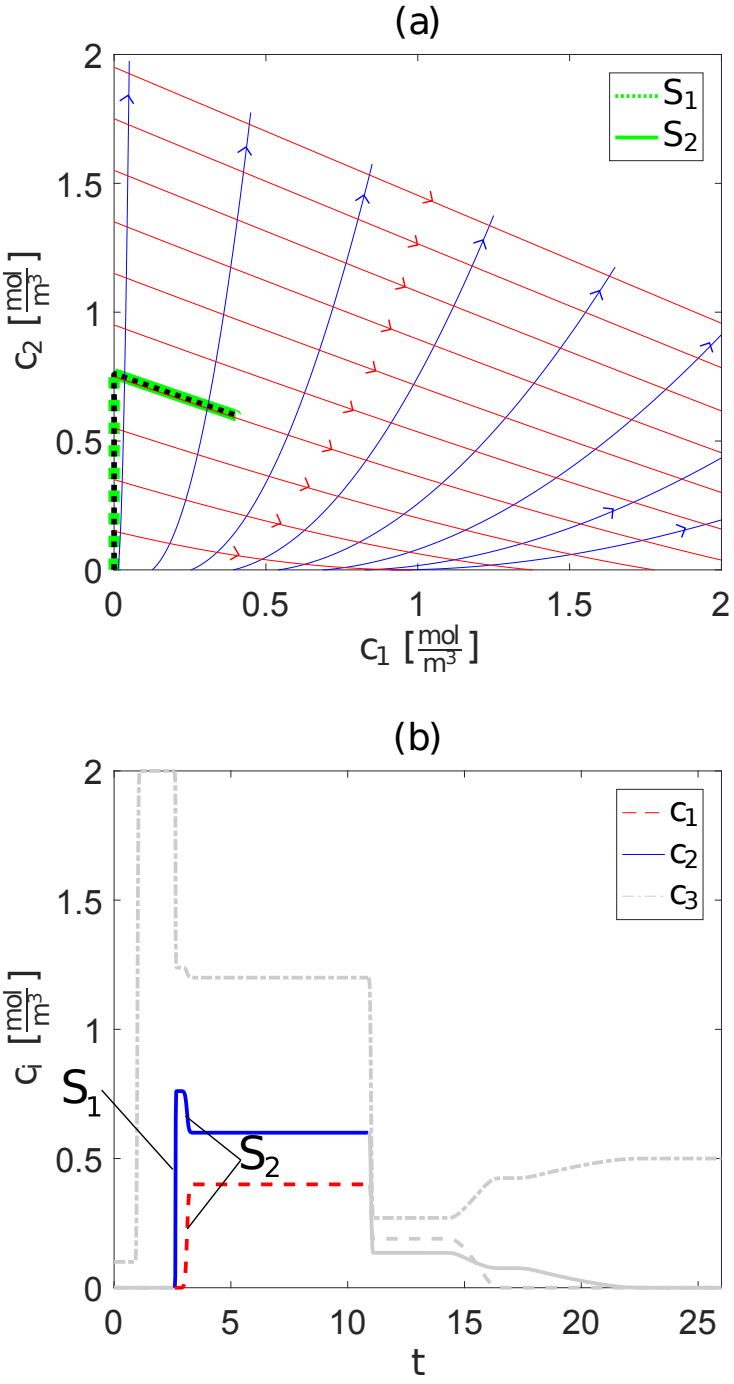

Figure 3: (a) Projection of the loading phase of the chromatographic cycle on the $c_{tot} = 2\ \frac{mol}{m^3}$ plane into the c_1, c_2 space. Numerical results (black dashed line) overlap the two shocks predicted by the equilibrium theory (green lines) and are identical to the corresponding ones in Fig. 1a. (b) Corresponding elution profile $c_i(t)$ indicating the two occurring shocks S_1, S_2 during the loading phase, which are identical to Fig. 1b.

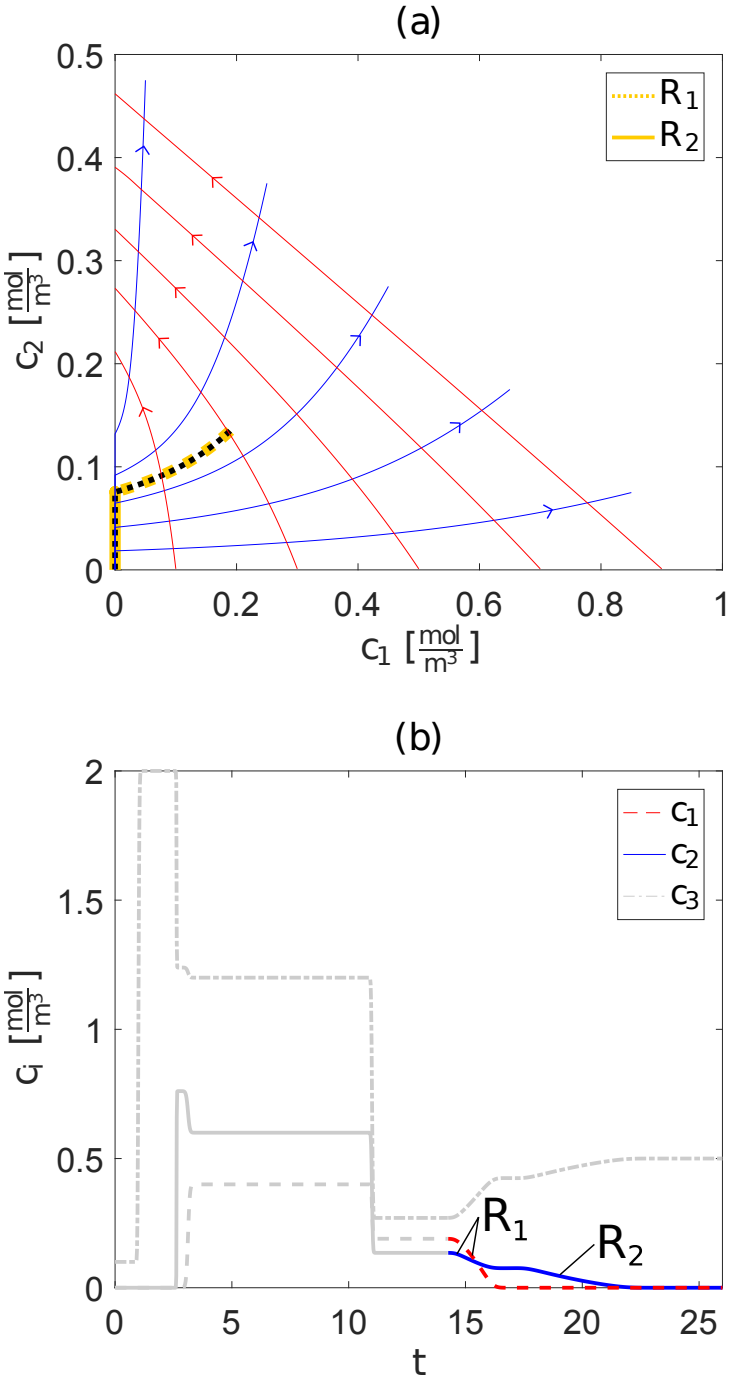

Figure 4: (a) Projection of the regeneration phase of the chromatographic cycle on the $c_{tot} = 0.5\ \frac{mol}{m^3}$ plane into the c_1, c_2 space. Numerical results (black dashed line) overlap the two spreading waves predicted by the equilibrium theory (orange lines). (b) Corresponding elution profile $c_i(t)$ during regeneration indicating two occurring spreading waves R_1, R_2 that show reversed selectivity compared to Fig. 1b.

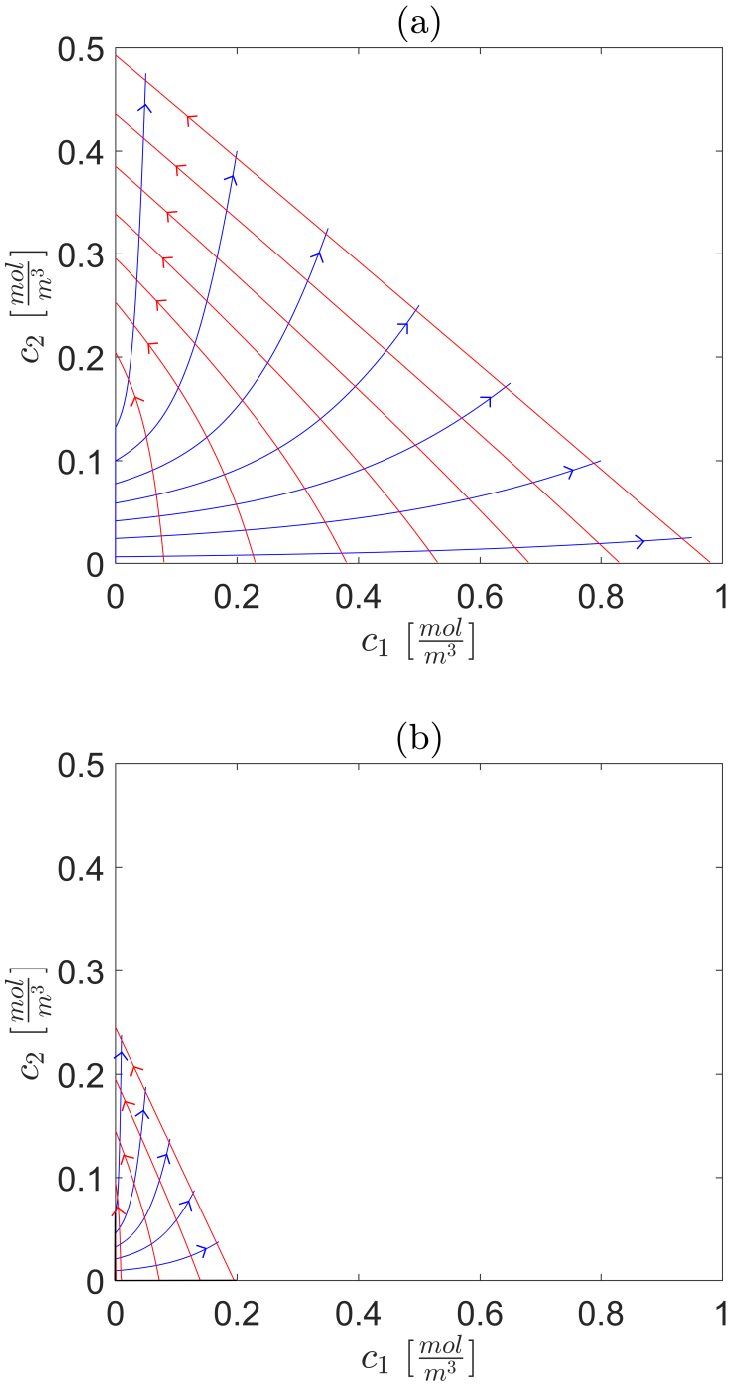

Figure 5: (a) Projection of the stoichiometric c_{tot}^{I} plane into the c_1, c_2 space, which is identical to Fig. 4a. (b) Projection of the steric c_{tot}^{II} plane into the c_1, c_2 space using the same domain as in (a).

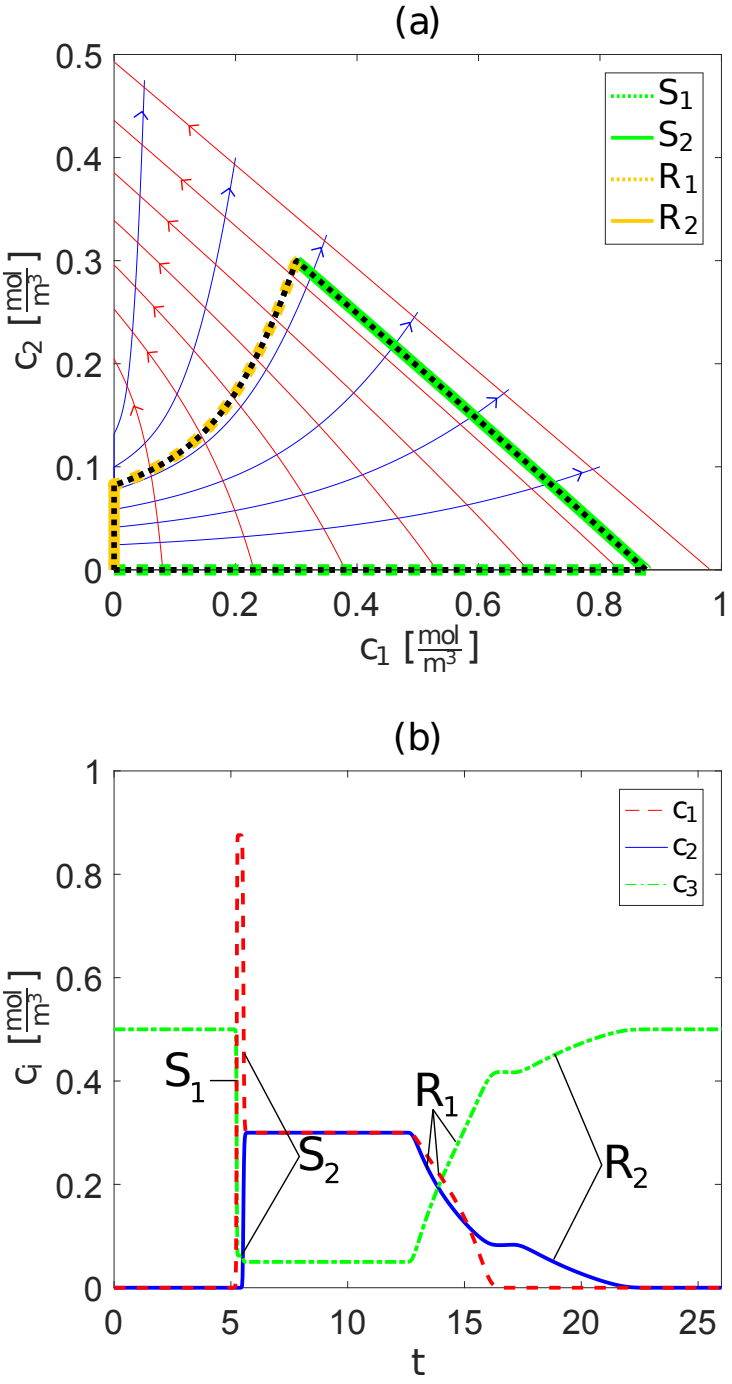

Figure 6: (a) Projection of the chromatographic cycle on the c^I_{tot} plane into the c_1, c_2 space realized by a pulse experiment of the classical stoichiometric ion exchange with constant solution normality c^I_{tot}. Numerical results (black dashed line) overlap solution predicted by the equilibrium theory (green and orange lines). (b) Corresponding elution profile $c_i(z)$ indicating two shocks S_1, S_2 and two spreading waves R_1, R_2.

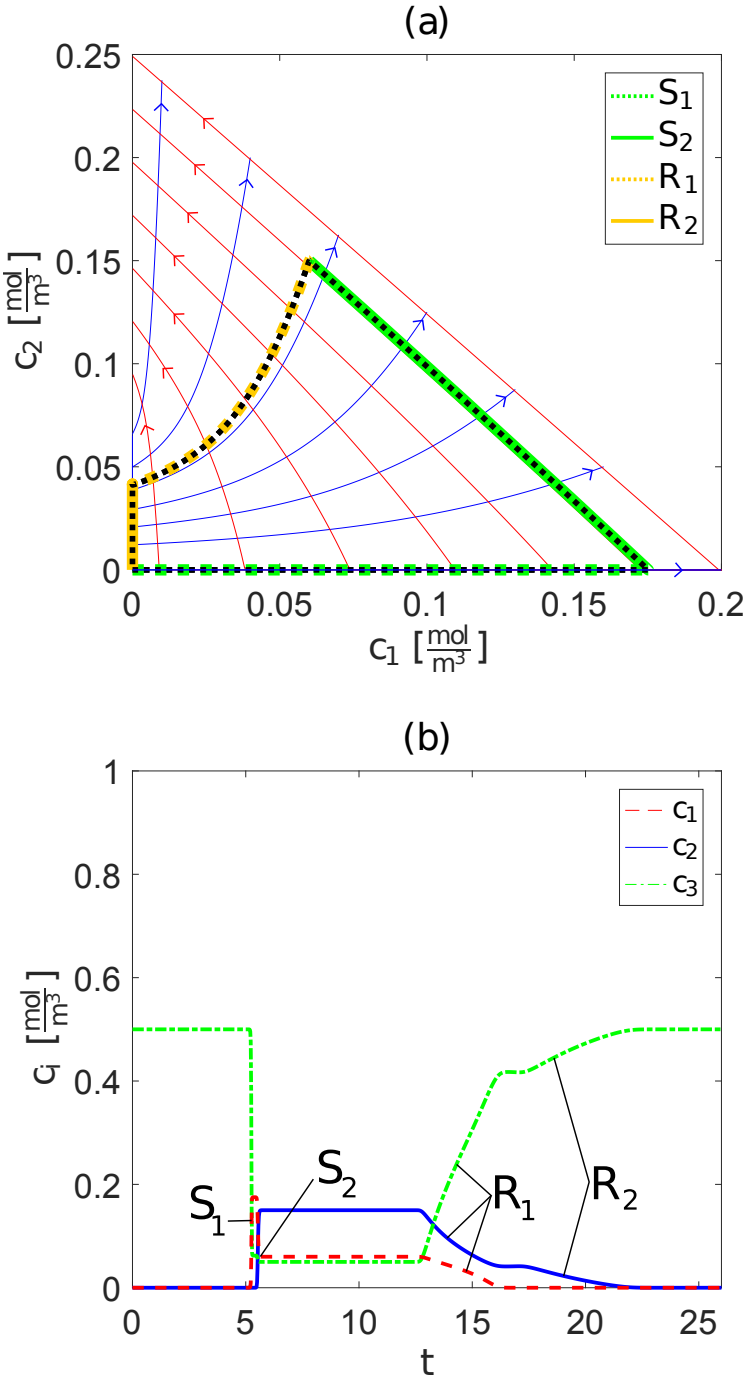

Figure 7: (a) Projection of the chromatographic cycle on the c_{tot}^{II} plane into the c_1, c_2 space realized by a pulse experiment of the ion exchange with steric hindrance and constant modified solution normality c_{tot}^{II}. Numerical results (black dashed line) overlap solution predicted by the equilibrium theory (green and orange lines). (b) Corresponding elution profile $c_i(z)$ indicating two shocks S_1, S_2 and two spreading waves R_1, R_2 qualitatively identical to Fig. 6b.

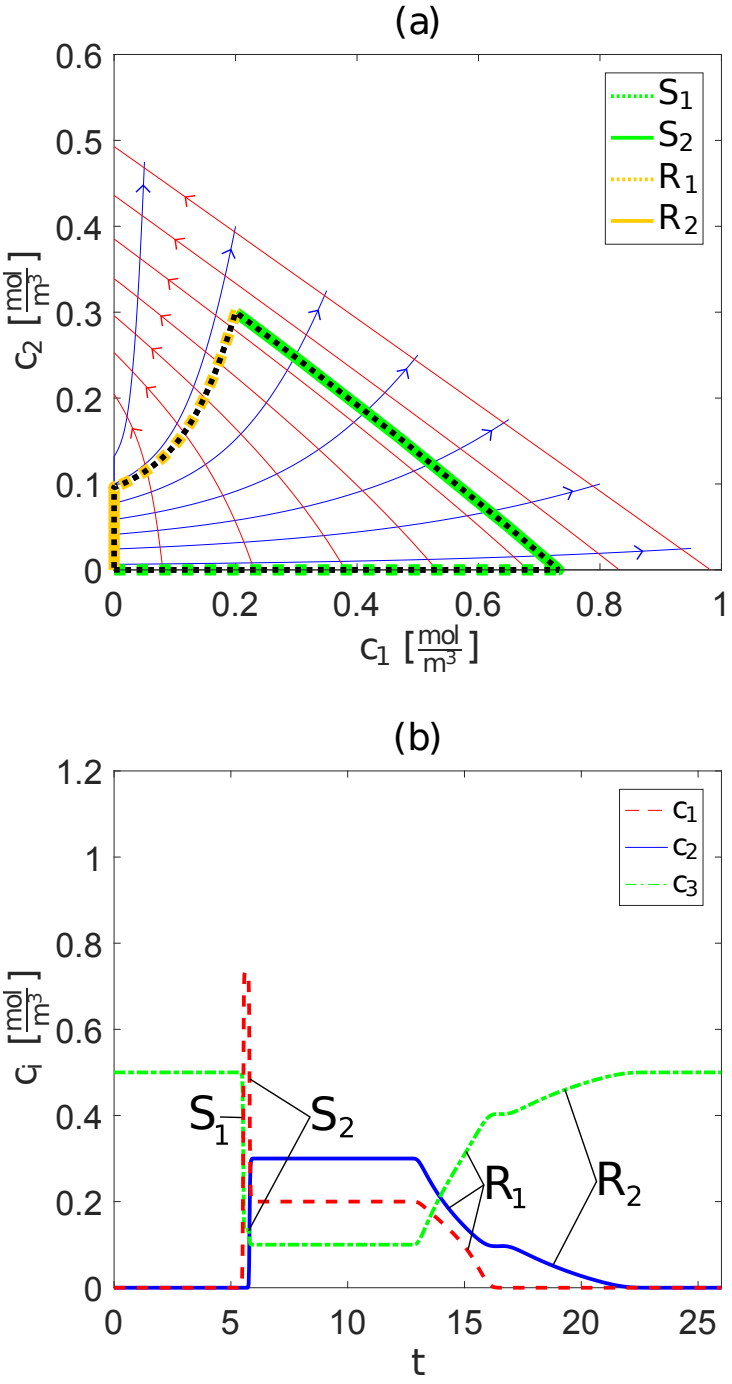

Figure 8: (a) Projection of the chromatographic cycle on the $c_{tot}^I = 0.5\ \frac{mol}{m^3}$ plane into the c_1, c_2 space realized by a pulse experiment of the classical stoichiometric ion exchange with constant solution normality c_{tot}^I. Numerical results (black dashed line) overlap solution predicted by the equilibrium theory (green and orange lines). (b) Corresponding elution profile $c_i(z)$ indicating two shocks S_1, S_2 and two spreading waves R_1, R_2 similar to Fig. 6b.

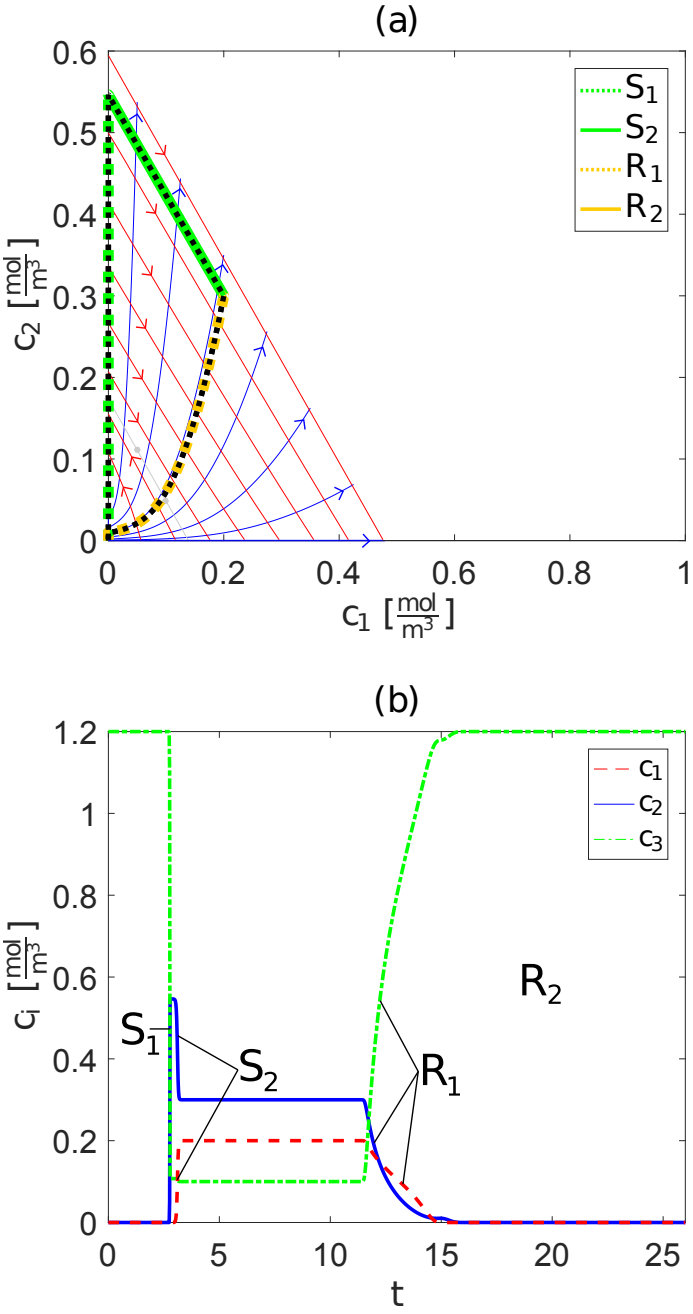

Figure 9: (b) Projection of the chromatographic cycle on the $c_{tot}^{II} = 1.2\ \frac{mol}{m^3}$ plane into the c_1, c_2 space realized by a pulse experiment of the ion exchange with steric hindrance and constant modified solution normality c_{tot}^{II}. The gray line indicates a $1,2$ selectivity reversal. Numerical results (black dashed line) overlap solution predicted by the equilibrium theory (green and orange lines). (d) Corresponding elution profile $c_i(z)$ indicating two shocks S_1, S_2 and two spreading waves R_1, R_2 with reversed selectivity of the two components compared to Fig. 8b.

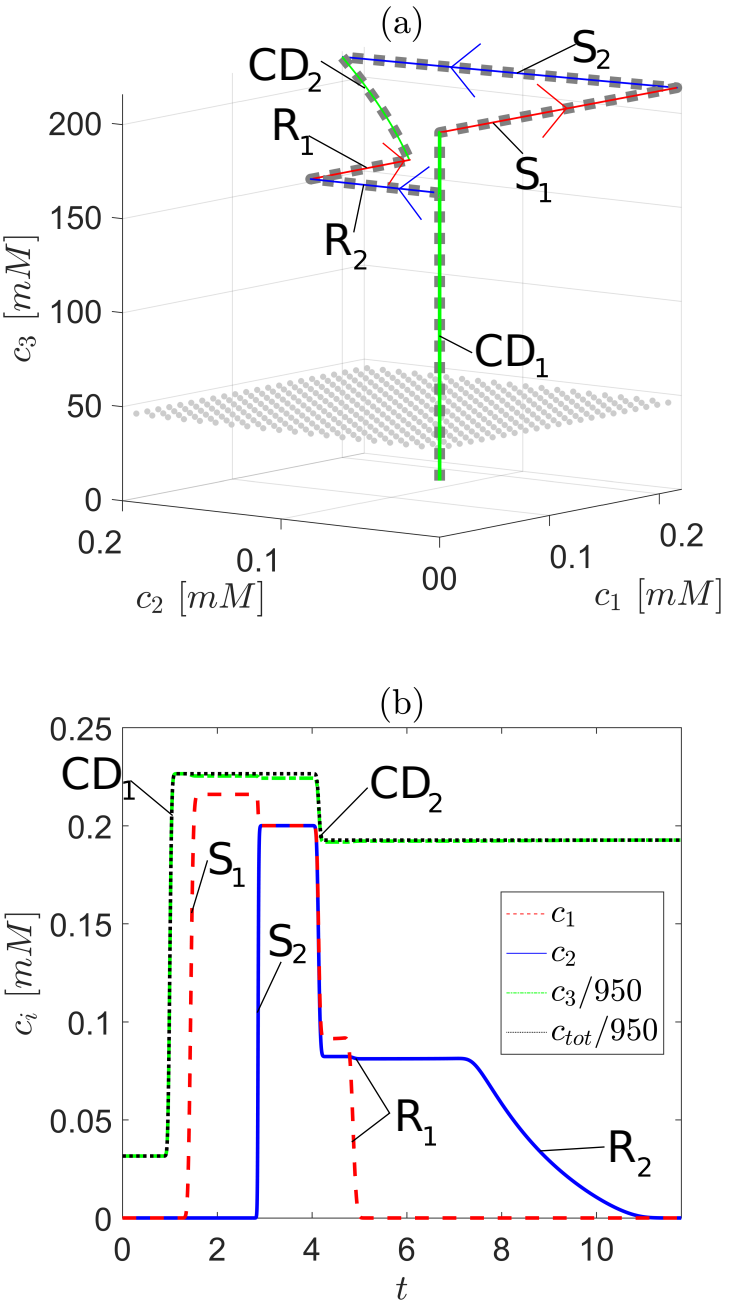

Figure 10: (a) Chromatographic cycle in the concentration phase space realized by a pulse experiment for two proteins (α-Chymotrypsinogen A, Cytochrome c) and sodium phosphate. Gray plane indicates reversal plane '1, 2'. Numerical results (gray dashed line) overlap two contact discontinuities, two shock curves and two integral curves, which are all predicted by the equilibrium theory (colored). (b) Corresponding elution profile $c_i(z)$ indicating that shocks and spreading waves take place for different but constant c_{tot} values. The values for c_3 and c_{tot} are scaled by a factor of $\frac{1}{950}$.